

CONFIDENTIAL

Copy 6
RM L56C23a

C.2



RESEARCH MEMORANDUM

FLIGHT INVESTIGATION AND ANALYSIS
OF THE WING DEFORMATIONS ON A SWEEP-WING BOMBER
DURING ROLLING MANEUVERS

By Alton P. Mayo and John F. Ward

Langley Aeronautical Laboratory
Langley Field, Va.

CLASSIFICATION CHANGED

LIBRARY COPY

UNCLASSIFIED

OCT 24 1956

LANGLEY AERONAUTICAL LABORATORY
LIBRARY NACA
LANGLEY FIELD, VIRGINIA

To: *Naval Research & Development*
By: *4 RN-120* *9-13-57*
Authority of: *NIS 10-8-57*
CLASSIFIED DOCUMENT

This material contains information affecting the National Defense of the United States within the meaning of the espionage laws, Title 18; U.S.C., Secs. 793 and 794, the transmission or revelation of which in any manner to an unauthorized person is prohibited by law.

NATIONAL ADVISORY COMMITTEE
FOR AERONAUTICS

WASHINGTON

October 19, 1956

CONFIDENTIAL

NACA RM L56C23a

NATIONAL ADVISORY COMMITTEE FOR AERONAUTICS

RESEARCH MEMORANDUM

FLIGHT INVESTIGATION AND ANALYSIS
OF THE WING DEFORMATIONS ON A SWEEP-WING BOMBER
DURING ROLLING MANEUVERS

By Alton P. Mayo and John F. Ward

SUMMARY


The results of deflection measurements made at six spanwise stations on the wing of a swept-wing jet bomber (Boeing B-47A) during rolling maneuvers are presented in the form of coefficients expressing the deflections due to the aileron loads, the sideslip loads, the wing-flapping inertia loads, and the rolling-velocity loads on the airplane. The procedures used to obtain the coefficients are presented along with comparisons of the experimental deflections and twists with those obtained from theoretical calculations. Comparisons of measured and computed deflections using available methods indicate good agreement. Detailed explanations of the least-squares procedures used in the analysis of the flight data and the methods used in the theoretical calculations are given in the appendixes.

INTRODUCTION

The design of a high-aspect-ratio swept-wing structure requires not only the application of advanced methods of stress analysis and the determination of the wing stiffness, but also the determination of aerodynamic and inertia spanwise load distributions that would occur under specified flight conditions. In each field the computations are not only lengthy but are subject to a sufficient number of assumptions so that the end result obtained when the results of the separate fields are combined are sometimes in doubt.

In order to secure an indication on the accuracy obtainable in each field, as well as of the accuracy of the end results, an extensive research program was undertaken in which a Boeing B-47A was used to obtain the experimental data.

In one phase of the research program, deflections of various surfaces were measured for the purpose of comparing the measured deflections with



computed values. Initial results on this phase have been given in references 1 and 2 which give the deflection influence coefficients for the wing and the analysis of the wing deflections obtained in symmetrical flight.

The present report is concerned mainly with the analysis of wing deflections obtained under unsymmetrical flight conditions. The unsymmetrical deflections were analyzed to obtain wing deflection coefficients expressing the deflections due to rolling velocity, aileron deflection, wing flapping, and sideslip. Comparisons are made between the experimentally determined deflections and those calculated theoretically. The procedures by which the flight data were analyzed for the various effects and the methods used in the theoretical calculations are given in the appendixes.

SYMBOLS

b'	wing span minus fuselage width, in. (fig. 3)
K_q	normal load factor at the tip of the rigid wing due to a unit pitching acceleration
K_p	normal load factor at the tip of the rigid wing due to a unit rolling acceleration
N	number of equations in least-squares solution
n	airplane normal load factor at airplane center of gravity, positive when inertia loads are downward ($n = 1$ in level flight)
n_T	normal load factor measured at the wing tip, positive when inertia loads are downward
n_{Tf}	normal load factor at wing tip due to wing flapping, positive when inertia loads are downward
p	airplane rolling angular velocity, positive for right roll, radians/sec
\dot{p}	airplane rolling angular acceleration, positive for increasing positive rolling velocity, radians/sec ²
\dot{p}_t	airplane rolling angular acceleration due to loads on horizontal and vertical tail, positive for increasing positive rolling velocity, radians/sec ²

q	airplane pitching angular velocity, positive for airplane nose pitching up, radians/sec
\dot{q}	airplane pitching angular acceleration, positive for increasing positive pitching velocity, radians/sec ²
X	streamwise distance from intersection of front spar center line and airplane center line, positive rearward, in. (fig. 3)
Y	lateral distance from airplane center line, positive left, in. (fig. 3)
Y'	lateral distance from airplane center line less one-half the fuselage width, positive left, in. (fig. 3)
Z''	vertical dimension, (measured from and perpendicular to the top of the fuselage) positive downward, in.
Z	total optigraph target deflection measured from wing-drooped position (ground zero), positive upward, in.
Z_i	target deflection due to wing inertia per unit airplane normal load factor, positive upward, in./n
$Z_{n\beta}$	target deflection per degree of sideslip at unit airplane normal load factor at the center of gravity, positive upward, in./deg
Z_{nT_f}	target deflection due to wing flapping, positive upward, in./n _{Tf}
Z_o	target deflection due to the wing airloads when the summation of the aerodynamic loads on the airplane is zero, positive upward, in.
Z_p	target deflection per unit airplane rolling velocity, positive upward, in./radian/sec
$Z_{\dot{p}}$	target deflection per unit airplane rolling acceleration, positive upward, in./radian/sec ²
Z_q	target deflection per unit airplane pitching velocity, positive upward, in./radian/sec
$Z_{\dot{q}}$	target deflection per unit airplane pitching acceleration, positive upward, in./radian/sec ²

Z_{roll}	target deflection due to combined unsymmetrical loadings associated with the rolling maneuver, positive upward, in.
Z'_{roll}	target deflection due to the combined unsymmetrical loadings plus the effect of the zero-lift loads and wing droop, positive upward, in.
$Z_{\delta\text{AIL}}$	target deflection per unit aileron deflection positive upward, in./deg
β	angle of sideslip, positive for right wing forward, deg
δ_{AIL}	left wing aileron deflection, positive downward, deg
α	wing section streamwise angle of attack, positive leading edge up, radians
$\alpha_{\delta\text{AIL}}$	wing streamwise angle of twist due to unit aileron deflection, radian/deg
$\alpha_{n_{T_f}}$	wing streamwise angle of twist due to unit wing flapping load factor, radian/ n_{T_f}
$\alpha_{n\beta}$	wing streamwise angle of twist due to unit sideslip angle, radian/ $n\beta$
α_p	wing streamwise angle of twist due to unit rolling velocity, radian/radian/sec

Matrix symbols:

$[\]$	row matrix
$\{ \ }$	column matrix
$[\]$	square matrix
$\ \ \ $	rectangular matrix
$[\]^{-1}$	inverse matrix
$[\]^{\circ}$	diagonal matrix

AIRPLANE AND TESTS

The airplane used in the test was a Boeing B-47A. (See figs. 1 and 2.) The changes in the test airplane configuration from the standard airplane were the installation of (1) an airspeed measuring boom and fairing on the nose and (2) an external canopy, housing the deflection-recording instruments, mounted atop the fuselage approximately at the intersection of the airplane center line and the wing 38-percent-chord line.

The flight-test data used in this paper pertain to four aileron-roll maneuvers flown during the B-47A flight research program conducted at the NACA High-Speed Flight Station at Edwards, Calif.

The four aileron-roll maneuvers consisted of left and right rolls at Mach numbers of 0.60 and 0.71. The specific values of aircraft weight, center-of-gravity position, Mach number, altitude, and dynamic pressure are included in table 1 for each roll maneuver.

INSTRUMENTATION AND ACCURACY

The instrumentation pertinent to the results presented in this paper consisted of a pitch turnmeter, roll turnmeter, yaw turnmeter, altimeter, airspeed recorder, an accelerometer at the center of gravity of the airplane, an accelerometer at the left wing tip, an aileron control-position recorder, a sideslip angle recorder, and an optigraph system for recording the wing deflections.

Corrections were made to the recorded center-of-gravity-accelerometer data for the small displacement from the airplane center of gravity. Corrections were made to the sideslip data for the effects of yawing velocity and induced flow. The induced-flow effects were small, that is, on the order of 5 percent, and were based on estimates of the flow around the fuselage and boom. All instruments used were of the standard NACA photographically recording type with the exception of the optigraph system which was designed especially for the complete test program on the airplane.

The wing optigraph system consisted of eight target lamps on the left wing and optical recording instruments located atop the fuselage approximately at the intersection of the 38-percent-chord line and the center line of the fuselage. (See fig. 3.) To facilitate recording the deflections optically in the daylight, high-intensity infrared light sources were used in combination with infrared sensitive recording film. The optigraph system was calibrated through the use of a calibration stick, with 12 lamps on it at 6-inch intervals, held vertically at each target station during

the calibration. All inflight measurements were made with reference to the wing-droop position with the airplane on the ground and with the outrigger gear clear.

The instrument sensitivities, locations, and the estimated accuracies of measurement are given in table 2.

METHOD AND RESULTS

In a maneuver combining pitching, yawing, and rolling, the final load distribution may be considered as arising from the superposition of various types of load distributions. In the analysis of the flight data and in the theoretical calculations of this paper, the final load distribution is considered as having the eight components enumerated subsequently. The wing structural deflections are assumed to be linearly related to these component load distributions. The following symmetrical distributions are considered:

- (1) A zero lift aerodynamic loading at zero airplane load factor necessary to balance fuselage and tail loads. The shape of this distribution is affected by actual geometric wing twist as well as by twist due to the interference effects of the fuselage and nacelles.
- (2) An additional type of load distribution proportional to airplane load factor. This distribution has aerodynamic and inertia subcomponents.
- (3) An airload distribution associated with pitching velocity which is a result of the wing-angle-of-attack change caused by the velocity of the wing perpendicular to the airstream.
- (4) A loading associated with the angular acceleration in pitch - mainly an inertia loading.

The following unsymmetrical distributions are considered:

- (5) A load distribution which is due to rolling velocity and which has aerodynamic and inertia subcomponents. The aerodynamic subcomponent is a result of the wing-angle-of-attack change caused by the velocity of the wing perpendicular to the airstream. The inertia subcomponent is a result of the airplane rolling acceleration associated with the rolling-velocity aerodynamic load.
- (6) A load distribution which is due to aileron deflection and which has aerodynamic and inertia subcomponents. The inertia subcomponent is a result of the airplane rolling acceleration caused by the aileron airload.

(7) A load distribution which is due to sideslip and which also has aerodynamic and inertia components. The inertia component is a result of the airplane rolling acceleration caused by the sideslip airloads.

(8) A load distribution which is due to wing flapping - mainly an inertia distribution; for this airplane the distribution has the frequency of the wing first unsymmetrical bending mode.

Analysis of Flight Data

In order to illustrate the type of flight data used in the analysis, time histories of the deflection of target 9 and the associated airplane motions are shown in figures 4, 5, 6, and 7 for the four roll maneuvers investigated.

The procedure by which such measurements were reduced to coefficients expressing the deflection at a point due to the various types of loads is as follows: In the range where wing section lift and pitching moment due to aileron are linear, the wing deflections caused by the aileron aerodynamic-plus-inertia load component (item 6) may be expressed as

$$Z = Z_{\delta_{AIL}} \delta_{AIL} \quad (1)$$

Also, from consideration of the loads involved, the wing aerodynamic-plus-inertia deflections caused by the rolling velocity (item (5)) of the airplane may be expressed as

$$Z = Z_p p \quad (2)$$

The deflection due to wing flapping (item (8)) is a result of an inertia effect and may be expressed as

$$Z = Z_{n_{T_F}} n_{T_F} \quad (3)$$

The load factor n_{T_F} at the wing tip caused by wing flapping was obtained from the load factor measured at the wing tip by eliminating the effect of the airplane center-of-gravity normal load factor and the effect of rolling and pitching acceleration. This is expressed as

████████████████████

$$n_{T_f} = n_T - (n + K_p \dot{p} + K_q \dot{q}) \quad (4)$$

where the expression within parentheses represents the computed normal acceleration at the wing tip for the rigid airplane. Time histories of the load factor n_{T_f} computed from equation (4) are also shown in figures 4, 5, 6, and 7.

Since for a given sideslip angle, the sideslip loading is related mainly to the effects of wing deflection and wing angle of attack, both of which are linearly related to the airplane normal load factor, (see appendix B) the deflection due to sideslip (item (7)) may be expressed as

$$Z = Z_{n\beta} n\beta \quad (5)$$

If the effects of aileron, rolling velocity, wing flapping, and sideslip are combined, the deflection at any point resulting from the unsymmetrical loading only can be expressed by the equation

$$Z_{\text{unsym}} = Z_{\delta_{AIL}} \delta_{AIL} + Z_{n_{T_f}} n_{T_f} + Z_{n\beta} n\beta + Z_p p \quad (6)$$

From equation (4) of reference 2, the deflections resulting from the symmetrical loadings may similarly be expressed as

$$Z_{\text{sym}} = Z_0 + Z_n n + Z_{\dot{q}} \dot{q} + Z_q q + Z_i \quad (7)$$

By adding the deflections due to equations (6) and (7), the total inflight deflections due to both the symmetrical and antisymmetrical loadings becomes

$$Z = (Z_0 + Z_i) + Z_n n + Z_{\dot{q}} \dot{q} + Z_q q + Z_{\delta_{AIL}} \delta_{AIL} + Z_{n_{T_f}} n_{T_f} + Z_{n\beta} n\beta + Z_p p \quad (8)$$

In the analysis of the roll maneuvers contained herein the unsymmetrical part of the deflections was isolated from the total measured

deflections by removing the effects of the normal load factor and pitching angular acceleration and velocity through the use of all but one of the symmetrical deflection coefficients already derived in reference 2. The symmetrical zero-lift and droop deflections $Z_0 + Z_1$ were not removed from the flight data because the factors which affect the zero-lift and droop deflections, such as temperature and possible slippages, were suspected to vary from flight to flight. The deflections due to the roll effects plus zero lift and droop were thus obtained from the flight data by the equation

$$Z'_{\text{roll}} = Z - Z_n n - Z_{\dot{q}} \dot{q} - Z_q q \quad (9)$$

During each run the Mach number, dynamic pressure, weight, and center-of-gravity position were held effectively constant. Thus, for each target in each run the residual deflections, after removing the symmetrical portion, may be represented in matrix notation by the equation

$$\begin{aligned} \left\{ Z'_{\text{roll}} \right\} &= (Z_0 + Z_1) \left\{ 1 \right\} + Z_{\delta_{\text{AIL}}} \left\{ \delta_{\text{AIL}} \right\} + \\ &Z_{n_{T_f}} \left\{ n_{T_f} \right\} + Z_{n_{\beta}} \left\{ n_{\beta} \right\} + Z_p \left\{ p \right\} \end{aligned} \quad (10)$$

where the columns $\left\{ \right\}$ on the right-hand side of equation (10) are corresponding measured values of δ_{AIL} , n_{T_f} , n_{β} , and p read from the flight records at 0.1-second intervals during the run. The coefficients $Z_0 + Z_1$, $Z_{\delta_{\text{AIL}}}$, $Z_{n_{T_f}}$, $Z_{n_{\beta}}$, and Z_p for each run were solved for by the method of least squares (see appendix A); approximately 50 data points per run were used.

The typical time-history plot of the Z'_{roll} deflections given in figure 8 shows the 51 points used in the analysis of the roll deflections of target number 9 in flight 10, run 17. Also plotted in figure 8 are the 51 data points for the total deflections of target number 9 measured during the roll.

The values of $Z_0 + Z_1$, $Z_{\delta_{\text{AIL}}}$, $Z_{n_{\beta}}$, $Z_{n_{T_f}}$, and Z_p coefficients calculated for each target in each run are presented in tables 3, 4, 5,

6, and 7, respectively. Table 8 lists the deflection coefficients for each target, the standard error of the coefficients, and the standard error of the equation for each target calculated by the method of appendix A for one typical run, that is, run 17 of flight 10. In the tables no results are shown for optigraph targets numbers 15 and 16 because the effects of roll on the total deflection of these targets were too small to permit a breakdown into the various coefficients.

Spanwise plots of the wing deflections caused by a unit aileron deflection are shown in figure 9. Similar spanwise plots for the wing deflection due to wing flapping, sideslip, and rolling velocity are shown in figures 10, 11, and 12, respectively. The variation of these wing deflections with dynamic pressure is shown in figure 13.

A comparison of the measured wing deflections and those calculated from the derived deflection coefficients obtained from the flight data is shown in figure 14 for flight 10, run 17.

Theoretical Calculations and Comparisons

With Flight Data

In the determination of the theoretical curves of wing deflection and twist for comparison with experimental results the methods of reference 3 were used to calculate the loads acting in each case. The lift-curve slopes used in the theoretical calculations were determined with data obtained from reference 4. The wing structural stiffness distributions were obtained from references 5 and 6. The wing deflections resulting from the application of the theoretically calculated loads were obtained through the structural influence coefficients of reference 1. The theoretical wing twist was calculated by using the theoretical structural matrices calculated by the methods of reference 3. A detailed outline of the theoretical calculations is given in appendix B.

Since wing deflections due to unsymmetrical loads are not very large as compared to the symmetrical deflections, it was deemed unnecessary to obtain experimental and theoretical variations of the various unsymmetrical deflection coefficients with dynamic pressure and Mach number. As a result, the analysis was confined to four roll maneuvers from which only one run was selected for comparison with theoretical calculations for the same flight condition.

Comparisons are made in figures 15 to 19 between experimental and theoretically calculated deflections and twist due to the aileron loads, the wing-flapping inertia loads, the sideslip loads, and the rolling-velocity loads on the airplane. The comparisons made pertain to a Mach number of 0.71, altitude of approximately 35,000 feet, and gross weight of 122,000 pounds which are the flight conditions of run 17 of flight 10.

The comparisons between calculated and experimental deflections due to the aileron are shown in figure 15. The deflections due to the theoretical aerodynamic load are also shown so as to give an indication of the magnitude of the aerodynamic deflections, the inertia deflections, and the sum.

The theoretical and experimental wing deflections due to wing flapping are shown in figure 16. The data points shown are the peak deflections when the maximum amplitude of the load-factor variation caused by wing flapping is unity at the wing-tip accelerometer. The theoretical points, as explained in appendix B, are the double integral of the assumed accelerations due to wing flapping. Examination of the equations of appendix B shows that good agreement between theoretical and experimental deflections for those stations inboard of the tip station is a result of the assumption made that the inertia distribution due to wing flapping was the same shape as the deflection curve due to wing flapping.

The forces on the airplane resulting from aileron deflection and wing flapping are generated solely by the wing, but in the case of sideslip and rolling velocity there are additional forces on the airplane generated by the tail. In the calculation of wing deflections due to sideslip and rolling velocity, account was made of the inertia deformations caused by the rolling acceleration resulting from the tail loads.

The experimental and theoretical deflections due to the effects of sideslip are given in figure 17. Shown in figure 17 are the deflections caused by the sideslip aerodynamic loads on the wing, the deflections caused by the aerodynamic plus inertia loads on the wing, and the total wing deflections due to sideslip on the wing and tail. In the theoretical calculations the effects of the sideslip loads on the fuselage and nacelles were neglected.

The comparison between the theoretical and experimental wing deflections due to rolling velocity is shown in figure 18. In a similar manner to that of figure 17, the theoretical wing deflections due to the rolling-velocity wing aerodynamic loads are shown along with the wing deflections due to the aerodynamic plus inertia forces in order to give indication as to the magnitude of the forces acting. The deflection caused by the rolling-velocity loads on the tail is also implicitly shown in the figure. In the calculation of the loads on the tail (see appendix B), the tail was assumed to roll about axis of intersection of the horizontal and vertical tail. The calculated effects of the tail loads are considered to be at the maximum since no corrections were made for interference effects on the tail. The effect of fuselage and nacelle loads on the rolling-velocity deflections was also neglected. All of these effects would tend to reduce the rolling moment and therefore the wing deflections.

The experimental and theoretical wing twist due to the various types of wing loadings are shown in figure 19. The methods by which these twists were obtained are outlined in appendix B.

DISCUSSION

Deflection Coefficients

It may be seen from figures 9 to 12 that the deflection coefficients, for various wing loads, when plotted against span position for each of the spars form well-defined curves. Inasmuch as that the deflection coefficients of each target were determined independently of the others, the smoothness of the curves indicates that equation (10) which was chosen to represent the data probably includes all of the important variables. The validity of equation (10) is also substantiated by the agreement shown in figure 14 between the measured deflections and the deflections calculated using the deflection coefficients and the measured airplane motions.

The final selection of variables in equation (10) was decided upon after first eliminating some of the variables of lesser importance. For example, terms expressing deflections due to yawing velocity, sideslip effects on the deflected aileron, and the independent effects on the fuselage and tail were originally included in equation (10). It was found that not only was the influence of these components small but also the standard errors for these additional coefficients were in some cases as large as the coefficients. For the maneuvers considered, the primary variables in equation (10) are aileron deflection and wing flapping; sideslip and rolling-velocity effects were found to be secondary.

The $Z_0 + Z_1$ coefficients of table 3 obtained from the maneuvers analyzed in this report are of the same magnitude as those presented in reference 2. The small differences which occur between the two sets of data are, as previously mentioned, thought to be attributable to small differences in slippages and temperature effects. Theoretical calculations, plots of the spar deflections, and variations with dynamic pressure are not presented for the symmetrical $Z_0 + Z_1$ coefficients because they are already covered in reference 2.

The deflections due to aileron and sideslip (shown in figs. 13(a) and 13(c)) decrease with decreasing dynamic pressure and tend toward a value of zero at zero dynamic pressure. This trend is expected since the major variable affecting the deflections in each case is the dynamic pressure.

In figure 13(b), the wing-flapping deflections are shown to be independent of dynamic pressure. This fact is true because the inertia forces are mainly causing these deflections.

If the effects of Mach number and flexibility are neglected, the wing loads due to unit rolling velocity are theoretically linearly related to the square root of dynamic pressure. Thus, the variation with dynamic pressure shown in figure 13(d) is somewhat expected. The difference shown in the figure between the deflections of a right roll and a left roll is a centrifugal effect which is explained by considering that in a left roll the left wing deflections due to both the rolling-velocity airloads and centrifugal loads are positive and in a right roll the airload deflections are negative and the centrifugal deflections are positive. Because of the low-slung nacelles and high wing of the B-47A, calculations indicate that for any reasonable vertical location of the axis of roll the overall effect of the centrifugal forces is to bend both right and left wing upward.

Theoretical Calculations and Comparisons

In general, the theoretical methods predicted the experimental deflections very well; however, the better agreements between experimental data and theory were obtained for the deflections due to the aileron deflection and wing flapping which involved only wing forces and which were previously mentioned as the most predominate deflections in the roll maneuvers. In the case of sideslip and rolling velocity, fuselage and tail effects which are difficult to calculate accurately tend to cause more disagreement between theoretical calculations and experimental data.

In the case of the wing deflections due to the aileron, the agreement between experiment and theory is good both for vertical deflections and wing twist. For wing flapping the vertical deflections are in agreement; but the twist is only in fair agreement for the inboard stations, and there is a large disagreement at the outboard stations. This behavior is believed to be due to the fact that the pitching oscillations of the combined outboard nacelle and wing, which are caused by the flapping of the wing, were not included in the theoretical twist calculations.

The deviations of the experimental data from the theoretical sideslip deflections, shown in figure 17, are suspected to be mainly a result of the faulty assumptions in the theoretical calculations since the experimental sideslip deflections (table 6) are of good behavior and are consistently about the same magnitude for all of the runs. As the equations for the sideslip effects used (see appendix B) are only approximations to a difficult problem, small disagreements can be expected. Also no account was taken in the theory for sideslip loads on the fuselage and the nacelles, both of which would affect the theoretical answers. In figure 19, the

experimental and theoretical twists due to sideslip tend to be in better agreement than do the vertical deflections shown in figure 17.

The experimental and calculated rolling-velocity deflections shown in figure 18 are in fair agreement. The small derivations shown are not surprising if the inability to accurately calculate tail loads and the neglect of nacelle aerodynamic loads are taken into consideration. The scatter in the experimental wing twists due to rolling velocity shown in figure 19(c) are probably a result of the small rolling deflections obtained in the flight maneuvers (that is, on the order of 1 in. at the wing tip).

CONCLUDING REMARKS

The inflight wing deformations on the B-47A airplane have been analyzed for the effects of the various types of wing loadings and the results are presented as deflection coefficients. Theoretical results combining existing methods of aerodynamics and stress analysis are also presented and show good agreement with the experimental data. Because of the particular aerodynamic and inertia characteristics of the Boeing B-47A wing, the wing deflections due to roll effects were relatively smaller than the symmetrical deflections previously reported in NACA RM L54K24a. Even though these deflections are small, a detailed analysis was possible due to the high measuring accuracy of the optigraph system.

Langley Aeronautical Laboratory,
National Advisory Committee for Aeronautics,
Langley Field, Va., March 13, 1956.

APPENDIX A

APPLICATION OF LEAST-SQUARES METHOD TO EVALUATING
DEFLECTION COEFFICIENTS

This appendix outlines the method used to reduce the wing deflections of this report to coefficient form. Since the method has a wider application, it is also illustrated in detail by obtaining numerical results for one of the time histories given in the body of the report.

The equation to which the least-squares methods are applied is equation (10) of the text, namely,

$$\begin{aligned} \left\{ Z'_{\text{roll}} \right\} &= (Z_0 + Z_1) \left\{ 1 \right\} + Z_{\delta_{\text{AIL}}} \left\{ \delta_{\text{AIL}} \right\} + \\ &Z_{n_{T_f}} \left\{ n_{T_f} \right\} + Z_{n\beta} \left\{ n\beta \right\} + Z_p \left\{ p \right\} \end{aligned}$$

where the columns, $\left\{ \right\}$, are corresponding values of Z'_{roll} , δ_{AIL} , n_{T_f} , $n\beta$, and p obtained from the flight records at various times during the run. Example values obtained from figure 5 and equation (9) for these columns are listed in the following table:

Time, sec	δ_{AIL} , deg	n_{T_f}	$n\beta$, deg	p , $\frac{\text{radian}}{\text{sec}}$	Z'_{roll} (from eq. (9))
0	-0.082	0.005	0.574	-0.004	23.144
1.0	-9.316	-.254	.658	-.146	19.719
2.0	-9.481	-.462	-.624	-.297	19.910
3.0	-6.986	-.016	-2.302	-.273	19.604
4.0	0	.517	-3.136	.038	21.274
5.0	-.415	.308	-.382	.082	21.818

When there are more equations than unknowns the equations must first be normalized in accordance with least-squares procedures given in reference 7. The normal equations from which a solution for the unknown deflection coefficients were obtained are as follows:

$$(Z_0 + Z_1)N + Z_{\delta_{AIL}} \sum \delta_{AIL} + Z_{n_{T_f}} \sum n_{T_f} + Z_{n\beta} \sum n\beta + Z_p \sum p = \sum Z'_{roll} \quad (A1)$$

$$(Z_0 + Z_1) \sum \delta_{AIL} + Z_{\delta_{AIL}} \sum \delta_{AIL}^2 + Z_{n_{T_f}} \sum n_{T_f} \delta_{AIL} + Z_{n\beta} \sum n\beta \delta_{AIL} + Z_p \sum p \delta_{AIL} = \sum Z'_{roll} \delta_{AIL} \quad (A2)$$

$$(Z_0 + Z_1) \sum n_{T_f} + Z_{\delta_{AIL}} \sum \delta_{AIL} n_{T_f} + Z_{n_{T_f}} \sum n_{T_f}^2 + Z_{n\beta} \sum n\beta n_{T_f} + Z_p \sum p n_{T_f} = \sum Z'_{roll} n_{T_f} \quad (A3)$$

$$(Z_0 + Z_1) \sum n\beta + Z_{\delta_{AIL}} \sum \delta_{AIL} n\beta + Z_{n_{T_f}} \sum n_{T_f} n\beta + Z_{n\beta} \sum (n\beta)^2 + Z_p \sum p n\beta = \sum Z'_{roll} n\beta \quad (A4)$$

$$(Z_0 + Z_1) \sum p + Z_{\delta_{AIL}} \sum \delta_{AIL} p + Z_{n_{T_f}} \sum n_{T_f} p + Z_{n\beta} \sum n\beta p + Z_p \sum p^2 = \sum Z'_{roll} p \quad (A5)$$

The value of N in the preceding equations is the number of sets of data available; in this example, six sets of data are available. In these equations the quantity $\sum \delta_{AIL}$ is simply the summation of the δ_{AIL} column in the preceding table. The quantity $\sum \delta_{AIL}^2$ is simply

the summation of the square of each number in the δ_{AIL} column. The quantity $\sum \delta_{AIL} n_{T_f}$ is obtained by multiplying, at each listed time, the value on the δ_{AIL} column by the corresponding value in the n_{T_f} column and summing all of the obtained products. A similar procedure is followed in determining all of the other summations in the preceding normal equations.

After the normal equations have been determined, the solution for the unknown coefficients $Z_0 + Z_1$, $Z_{\delta_{AIL}}$, $Z_{n_{T_f}}$, $Z_{n_{\beta}}$, and Z_p may be obtained. The normal equations for the example are

$$\begin{aligned} 6(Z_0 + Z_1) - 26.280Z_{\delta_{AIL}} + 0.098Z_{n_{T_f}} - \\ 5.212Z_{n_{\beta}} - 0.592Z_p = 125.469 \end{aligned} \quad (A6)$$

$$\begin{aligned} -26.280(Z_0 + Z_1) + 255.660362Z_{\delta_{AIL}} + 6.730032Z_{n_{T_f}} + \\ 15.979450Z_{n_{\beta}} + 6.048813Z_p = -520.374736 \end{aligned} \quad (A7)$$

$$\begin{aligned} 0.098(Z_0 + Z_1) + 6.730032Z_{\delta_{AIL}} + 0.640394Z_{n_{T_f}} - \\ 1.578110Z_{n_{\beta}} + 0.223588Z_p = 3.313612 \end{aligned} \quad (A8)$$

$$\begin{aligned} -5.212(Z_0 + Z_1) + 15.979450Z_{\delta_{AIL}} - 1.578110Z_{n_{T_f}} + \\ 16.431440Z_{n_{\beta}} + 0.569510Z_p = -106.342230 \end{aligned} \quad (A9)$$

$$\begin{aligned} -0.592(Z_0 + Z_1) + 6.048813Z_{\delta_{AIL}} + 0.223588Z_{n_{T_f}} + \\ 0.569510Z_{n_{\beta}} + 0.192238Z_p = -11.454072 \end{aligned} \quad (A10)$$

The preceding normalized equations were obtained from only six sets of data and are presented here only to demonstrate the method; actually the coefficients were determined from 51 sets of data in order to obtain more accurate values of the deflection coefficients. Further discussion is based on the normal equations obtained from 51 sets of data points for flight 10, run 17 of figure 5 as follows: The normal equations in this case were

$$\begin{aligned} 51(Z_0 + Z_1) - 233.831Z_{\delta_{AIL}} + 3.066Z_{n_{Tf}} - \\ 55.327Z_{n_{\beta}} - 5.803Z_p = 1057.730 \end{aligned} \quad (A11)$$

$$\begin{aligned} -233.831(Z_0 + Z_1) + 2092.574223Z_{\delta_{AIL}} - 11.527022Z_{n_{Tf}} + \\ 116.807821Z_{n_{\beta}} + 54.017682Z_p = -4437.738398 \end{aligned} \quad (A12)$$

$$\begin{aligned} 3.066(Z_0 + Z_1) - 11.527022Z_{\delta_{AIL}} + 7.743859Z_{n_{Tf}} - \\ 8.139764Z_{n_{\beta}} - 0.447479Z_p = 47.507306 \end{aligned} \quad (A13)$$

$$\begin{aligned} -55.327(Z_0 + Z_1) + 116.807821Z_{\delta_{AIL}} - 8.139764Z_{n_{Tf}} + \\ 161.251305Z_{n_{\beta}} + 5.324052Z_p = -1185.655375 \end{aligned} \quad (A14)$$

$$\begin{aligned} -5.803(Z_0 + Z_1) + 54.017682Z_{\delta_{AIL}} - 0.447479Z_{n_{Tf}} + \\ 5.324052Z_{n_{\beta}} + 1.749173Z_p = -109.307618 \end{aligned} \quad (A15)$$

which when solved simultaneously give

$$(Z_0 + Z_1) = 23.047 \quad Z_{\delta_{AIL}} = 0.494 \quad Z_{n_{Tf}} = -2.218$$

$$Z_{n_{\beta}} = 0.163 \quad Z_p = -2.346$$

Substitution of the coefficients in equation (10) gives:

$$Z'_{roll} = 23.047 + 0.494Z_{\delta_{AIL}} - 2.218n_{T_f} + 0.163n_{\beta} - 2.346p \quad (A16)$$

The solution to the normal equations presented in this paper were obtained through the use of Crout's method (ref. 8), because it was easily applicable to computing-machine use.

An estimate of the ability of equation (A16) to fit the measured deflections is given by

$$\text{Standard error of fit} = \pm \sqrt{\frac{\sum (\text{dev})^2}{N - U}} \quad (A17)$$

where N equals the number of equations (51 in the case cited) and U equals the number of unknowns (5).

The summation of deviations squared term, $\sum (\text{dev}^2)$, was obtained from:

$$\begin{aligned} \sum \text{dev}^2 = & \sum (Z'_{roll})^2 - (Z_0 + Z_1) \sum Z'_{roll} - \\ & Z_{\delta_{AIL}} \sum Z'_{roll} \delta_{AIL} - Z_{n_{T_f}} \sum Z'_{roll} n_{T_f} - \\ & Z_{n_{\beta}} \sum Z'_{roll} n_{\beta} - Z_p \sum Z'_{roll} p \end{aligned} \quad (A18)$$

These summations are given for $N = 51$ in equation (A11) to (A15), with the exception of Z'_{roll}^2 which were obtained by summing the squares of the 51 values of Z'_{roll} . The standard error of fit for target 9 was ± 0.176 inch, which indicates that the average deviation of the measured deflection data points from the determined equation is approximately ± 0.176 inch.

The standard error of each of the coefficients was obtained by the equation

$$\left\{ \text{Standard error of coefficients} \right\} = (\text{Standard error of equation}) \left\{ \sqrt{C} \right\} \quad (A19)$$

The values of the \sqrt{C} coefficients were determined from the numbers in the matrix of the normal equation (A11) to (A15), as follows.

The normal equations (in matrix form) for the 51-point example presented previously are:

$$\begin{bmatrix} 51 & -233.831 & 3.066 & -55.327 & -5.803 \\ -233.831 & 2092.574223 & -11.527022 & 116.807821 & 54.017682 \\ 3.066 & -11.527022 & 7.743859 & -8.139764 & -0.447479 \\ -55.327 & 116.807821 & -8.139764 & 161.251305 & 5.324052 \\ -5.803 & 54.017682 & -0.447479 & 5.324052 & 1.749173 \end{bmatrix} \begin{Bmatrix} (Z_o + Z_i) \\ Z_{\delta_{AIL}} \\ Z_{n_{T_F}} \\ Z_{n_{\beta}} \\ Z_p \end{Bmatrix} = \begin{Bmatrix} 1057.730 \\ -4437.738398 \\ 47.507306 \\ -1185.655375 \\ -109.307618 \end{Bmatrix} \quad (A20)$$

or

$$[A] \begin{Bmatrix} Z_o + Z_i \\ Z_{\delta_{AIL}} \\ Z_{n_{T_F}} \\ Z_{n_{\beta}} \\ Z_p \end{Bmatrix} = \begin{Bmatrix} \sum Z'_{roll} \\ \sum Z'_{roll} \delta_{AIL} \\ \sum Z'_{roll} n_{T_F} \\ \sum Z'_{roll} n_{\beta} \\ \sum Z'_{roll} p \end{Bmatrix} \quad (A21)$$

The inverse of matrix $[A]$ is (giving only the diagonal elements)

$$[A]^{-1} = \begin{bmatrix} 0.0910146 & \text{-----} & \text{-----} & \text{-----} & \text{-----} \\ \text{-----} & 0.0048902 & \text{-----} & \text{-----} & \text{-----} \\ \text{-----} & \text{-----} & 0.1367970 & \text{-----} & \text{-----} \\ \text{-----} & \text{-----} & \text{-----} & 0.0164597 & \text{-----} \\ \text{-----} & \text{-----} & \text{-----} & \text{-----} & 3.7846045 \end{bmatrix} \quad (A22)$$

or

$$[A]^{-1} = \begin{bmatrix} c_{11} & --- & --- & --- & --- \\ --- & c_{22} & --- & --- & --- \\ --- & --- & c_{33} & --- & --- \\ --- & --- & --- & c_{44} & --- \\ --- & --- & --- & --- & c_{55} \end{bmatrix} \quad (A23)$$

Thus the standard error S of the coefficients denoted by the subscripts for this example were

$$\left\{ \begin{array}{l} S_{(Z_o+Z_i)} \\ S_{Z_{\delta_{AIL}}} \\ S_{Z_{nTf}} \\ S_{Z_{n\beta}} \\ S_{Z_p} \end{array} \right\} = (S_{\text{equation}}) \left\{ \begin{array}{l} \sqrt{c_{11}} \\ \sqrt{c_{22}} \\ \sqrt{c_{33}} \\ \sqrt{c_{44}} \\ \sqrt{c_{55}} \end{array} \right\} = \left\{ \begin{array}{l} \pm 0.053 \\ \pm 0.011 \\ \pm 0.065 \\ \pm 0.022 \\ \pm 0.342 \end{array} \right\} \quad (A24)$$

APPENDIX B

THEORETICAL DEFLECTION COEFFICIENTS

In the theoretical calculations presented in the body of the report the effects of the wing airload, the effects of the rolling acceleration due to the wing airloads, the fuselage airloads, and the airplane tail loads have to be considered. The general procedure was to calculate the wing airloads and the rolling acceleration resulting from these loads by the methods of reference 3 and, when necessary, to approximate the rolling acceleration due to the fuselage and tail loads by the methods included in this appendix.

SYMBOLS PERTINENT TO APPENDIX B

A'	amplitude of oscillation, in.
$C_{m_{\delta_{AIL}}}$	aileron-section pitching moment due to unit aileron deflection
g	acceleration due to gravity, 386.4 in./sec ²
I_x	airplane rolling moment of inertia, 490×10^6 lb-in. ² (obtained from ref. 9)
$K_{\delta_{AIL}}$	aileron-section effectiveness factor
m_o	wing-section lift-curve slope
r	spanwise distance to vortex center line, in.
S	total wing area, in. ²
V	true free-stream velocity, in./sec
α	wing-section streamwise angle of attack, positive leading edge up
t	time, sec
$\frac{d\alpha_w}{dn}$	wing-section total angle of attack per unit load factor

$\frac{d\theta_y}{dn}$ slope of elastic axis deflection curve per unit load factor

Λ wing sweep angle, positive for sweepback, deg

ω circular frequency of the wing flapping

Matrix notation:

$[A]$ structural matrix expressing the wing angle of twist caused by the nacelle pitching moment (ref. 3)

$[K_G]$ geometry matrix to determine rolling moment associated with known wing loads

$\{l\}$ wing-section lift, lb/in.

$\{S_{O_H}\}$ angle of attack induced on the wing due to the fuselage overvelocities caused by sideslip

$[S_1 + S_1]$ aerodynamic downwash matrix calculated from the geometry of the wing and fuselage vortices

$[S_2]$ structural matrix relating wing twist to the wing loads

$[1]$ diagonal matrix in which diagonal elements are equal to unity

$\{\alpha_g\}$ wing-section streamwise angle of attack in the flight condition due to all effects other than the angle of twist due to 0.25c airloads

$\{\alpha_{c_m \delta_{AIL}}\}$ wing-section angle of attack caused by wing twist due to aileron pitching moment caused by unit aileron deflection

$\{\alpha_p\}$ wing angle of attack caused by the rolling acceleration inertia deformations

$||\delta_l||$ structural matrix expressing the wing deflections due to the wing-quarter-chord loads

$\{\delta_p\}$ column matrix expressing the centrifugal deflection of the wing caused by a unit rolling velocity at $n = 1$

- $\{\delta_p\}$ structural matrix expressing target deflections per unit rolling acceleration
- $\{Z\}$ matrix of wing target deflections
- $\{n_F\}$ matrix of wing-flapping normal load factor at the optigraph targets, when $n_{T_F} = 1$
- q^* dynamic pressure

The theoretical unsymmetrical aerodynamic loads are given by equation (24) of reference 3 as

$$\left[\begin{bmatrix} 0 \\ 1 \end{bmatrix} - q^* S [A] \right] \begin{bmatrix} 0 \\ \frac{1}{4q^* m_0} \end{bmatrix} [S_1 + S_1] - [S_2] \{t\} = \{\alpha_g\} \quad (B1)$$

In order to account for rolling acceleration flexibility effects, where the rolling acceleration is a function of the airloads on the wing, the equation

$$[K_G] \{l\} = I_x \ddot{p} \quad (B2)$$

was solved simultaneously with equation (B1) so as to give the wing loads and the rolling acceleration associated with each flight condition.

The effective wing angles of attack $\{\alpha_g\}$ due to aileron, side-slip, and rolling velocity were determined separately and inserted in equation (B1) so that each solution gave the wing airload and the rolling acceleration resulting from that angle-of-attack distribution.

The wing bending and torsional stiffness distribution of references 5 and 6 were used in the determination of the structural matrices in equation (B1). The wing was treated as a cantilever beam fixed at the intersection of the wing 38-percent-chord line and the fuselage wall. The geometry and downwash matrices of the above equation were calculated for a vortex system of 10 vortices per semispan. The spanwise location of these vortices may be deduced from the twist comparison figure (fig. 19) where the theoretical twist data points are shown. The values of the section-lift-curve slopes m_0 were determined through the use of the above equation as applied to the wind-tunnel symmetrical data of reference 4 and includes correction to the Mach number by use of the Prandtl-Glauert equation.

In the determination of the aileron airload on the flexible wing

$$\{\alpha_g\} = \{K_{\delta_{AIL}}\} \delta_{AIL} + \{\alpha_p\} \dot{p}_{AIL} + \{\alpha_{cm\delta_{AIL}}\} \delta_{AIL} \quad (B3)$$

The aileron-section effectiveness factors, $\{K_{\delta_{AIL}}\}$ were obtained from reference 10. The matrix $\{\alpha_{cm\delta_{AIL}}\}$ was determined by using the values of $C_{m\delta_{AIL}}$ obtained from reference 6 in conjunction with the proper structural matrix determined by the method previously mentioned. The α_p column matrix was calculated by applying the rolling acceleration inertia distribution to the wing through theoretical structural matrices.

In the case of rolling velocity p , the equation

$$\{\alpha_g\} = \left\{ \frac{r}{V} \right\} p + \{\alpha_p\} \dot{p} \quad (B4)$$

again includes the effects of inertia on the flexible wing.

The sideslip $\{\alpha_g\}$ distribution was calculated as

$$\{\alpha_g\} = \left\{ \frac{d\alpha_w}{dn} \right\} \beta \tan \Lambda + \{S_{OH}\} \beta + \left\{ \frac{d\theta_y}{dn} \right\} \beta \cos \Lambda + \{\alpha_p\} \dot{p}_\beta \quad (B5)$$

which is the result of the flexible swept wing and fuselage sideslipping at $n = 1$ and which includes the effects of wing dihedral and fuselage overvelocities calculated by the methods of references 11, 12, and 13.

In the case of sideslip and rolling velocity, where the associated rolling acceleration of the airplane is affected by the tail loads, the wing deflection caused by the tail loads was handled separately and superimposed on wing effects to obtain the wing deflection due to the combined effects of wing and tail. The vertical-tail-load effect in sideslip was calculated by using a C_{L_β} of 0.045 (estimated from preliminary strain-gage data obtained in the Flight Research Division of the Langley Aeronautical Laboratory) and by assuming the rolling axis to be through the airplane center of gravity and parallel to the fuselage axis. The horizontal tail was assumed to act in the same manner

as the wing in sideslip. The angle of attack of the horizontal tail was calculated from the airplane tail-off pitching moment at $n = 1$.

In calculating the effect of tail load on rolling velocity deflections the tail was assumed to be rolling about an axis passing through the intersection of the vertical and horizontal tail. The wing c_l distribution due to rolling velocity was assumed to act on the tail.

Once the total airloads and rolling accelerations were determined for the flight condition, the theoretical-angle-of-attack change due to wing twist was calculated from the equation

$$\{\alpha\} = [S_2] \{l\} + \{\alpha_p\} \dot{p} \quad (B6)$$

In the case of wing twist due to aileron, an additional term $\{\alpha_{cm\delta_{AIL}}\} \delta_{AIL}$ was included in equation (B6) to account for wing twist due to aileron pitching moment.

In the calculation of the theoretical angle of twist due to wing flapping, an inertia distribution which had a value of unit load factor at the wing tip and was the shape of the wing-flapping deflection curve was applied to the wing through the use of a proper structural matrix calculated by the method previously mentioned. No account was taken of pitching oscillations of the wing or nacelle caused by wing flapping.

The deflections were determined from the equation

$$\{Z\} = \|\delta_l\| \{l\} + \{\delta_p\} \dot{p} \quad (B7)$$

where the matrices $\|\delta_l\|$ and $\{\delta_p\}$ were determined from the influence coefficients of reference 1.

The wing deflection due to aileron was calculated by using equation (B7) and altering the $\|\delta_l\|$ matrix to account for the shift in position of the lifting line from the quarter-chord line at the aileron in accordance with reference 14. A term $\{\delta_p\} p^2$ was added to equation (B4) in the calculation of rolling-velocity wing deflections, which accounted for the centrifugal effects on the deflected wing. In the

calculation of the $\{\delta_p\}$ matrix, the vertical location of the airplane center of gravity was assumed to be at $Z'' = 56$ inches, obtained from reference 9.

The deflections associated with wing flapping were theoretically checked by assuming sinusoidal oscillations and calculating the amplitude of oscillation from the equation

$$\frac{d^2 z}{dt^2} = A' \omega^2 \sin \omega t$$

or

$$n_f g = A' \omega^2 \sin \omega t$$

where ω was measured from the time-history plots of n_{T_f} . The spanwise shape of the wing acceleration distribution due to wing flapping n_f was assumed to be of the same shape as the wing deflection curve associated with n_f .

Thus, at the maximum amplitude where $\sin \omega t = 1$

$$\{Z\} = -\frac{g}{\omega^2} \{n_f\}$$

REFERENCES

1. Mayo, Alton P., and Ward, John F.: Experimental Influence Coefficients for the Deflection of the Wing of a Full-Scale, Swept-Wing Bomber. NACA RM L53L23, 1954.
2. Mayo, Alton P., and Ward, John F.: Flight Investigation and Analysis of the Wing Deformations of a Swept-Wing Bomber During Push-Pull Maneuvers. NACA RM L54K24a, 1955.
3. Gray, W. L., and Schenk, K. M.: A Method for Calculating the Subsonic Steady-State Loading on an Airplane With a Wing of Arbitrary Plan Form and Stiffness. NACA TN 3030, 1953.
4. Spangler, T. A.: The Span-Load Distribution of the XB-47 Wing. Document No. D-8055, Boeing Airplane Co., Dec. 24, 1946.
5. Parsons, Cecil E.: Wing Destruction Tests - Model B-47B. Test No. T-25299 (Contract No. W33-038 ac 22413), Boeing Airplane Co. (revised Apr. 14, 1951).
6. Payne, Alan: Wing Stress Analysis. [Models XB-47 and B-47A.] Document No. D-7740 (Contract Nos. W33-038 ac-8429 and ac-22413), Boeing Airplane Co., Aug. 14, 1947.
7. Whittaker, Edmond, and Robinson, G.: The Calculus of Observations. Fourth ed. Blackie & Son, Ltd. (London and Glasgow), 1944.
8. Crout, Prescott D.: A Short Method for Evaluating Determinants and Solving Systems of Linear Equations With Real or Complex Coefficients. Trans. Am. Inst. Elec. Eng., vol. 60, 1941, pp. 1235-1240.
9. Gray, E. Z., Sandoz, P., and Entz, H.: Design Load Criteria. [Model B-47B.] Vol. I. Document No. D-9441 (Contract No. W33-038 ac-22413), Boeing Airplane Co., Nov. 9, 1948.
10. Perkins, Courtland D., and Hage, Robert E.: Airplane Performance - Stability and Control. John Wiley & Sons, Inc., 1949.
11. Holtby, K., and Seiler, R.: Development of Lateral Controls for Flexible Swept Wings (Model B-47). Doc. No. D-9458, Contract Nos. W33-038 ac-8429 and W33-038 ac-22413, Boeing Airplane Co., Apr. 6, 1950.

12. Multhopp, H.: The Application of the Wing Theory to Problems of Flight Mechanics. Reps. and Translations No. 860, British M.A.P. Völkenrode, Dec. 15, 1946.
13. Glauert, H.: The Elements of Aerofoil and Airscrew Theory. Second ed., Cambridge Univ. Press, 1947. (Reprinted 1948.)
14. Nelson, Melvin A.: Wing Stress Analysis. [Model B-47B.] Vol. I. Document No. D-10207 (Contract No. W33-038 ac-22413), Boeing Airplane Co., Apr. 10, 1950.

TABLE 1.- FLIGHT CONDITIONS

Flight	Run	Maneuver	Mach number	Dynamic pressure, lb/sq ft	Altitude, ft	Aircraft weight, lb	Position of c.g., percent M.A.C.
8	15	Left roll	0.60	125	34,500	116,000	16.04
10	17	Left roll	.71	177	34,900	122,000	22.48
10	18	Right roll	.71	171	35,300	121,000	25.79
12	14	Right roll	.60	130	34,800	117,000	13.50

TABLE 2.- INSTRUMENT LOCATIONS, SENSITIVITIES, AND ACCURACIES

Instrument	Location			Sensitivity on recording film	Combined accuracy of instrumentation and reading
	X, in.	Y, in.	Z", in.		
Aileron-angle recorder	422	538	Upper wing surface	0.060 in./deg	$\pm 0.4^\circ$
Sideslip-angle recorder	-466	0	Vane 7 in. below boom	0.100 in./deg	$\pm 0.2^\circ$
Airplane-center-of-gravity accelerometer	241	27	94	0.987 in./n	± 0.010
Wing-tip accelerometer	485	684	Inside wing tip	0.304 in./n _T	± 0.025
Pitch-angular-velocity recorder . .	227	21	94	4.016 in./radian/sec	± 0.005 radian/sec
Pitch angular acceleration (a)	(a)	(a)	(a)	$45^\circ = 0.99$ radian/sec ²	± 0.01 radian/sec ²
Roll-angular-velocity recorder . . .	252	15	94	1.027 in./radian/sec	± 0.020 radian/sec ²
Roll angular acceleration (a)	(a)	(a)	(a)	$45^\circ = 0.25$ radian/sec ²	± 0.01 radian/sec ²
Optigraph target 9	474.5	681.0	Upper wing surface	0.0212 in./in.	± 0.2 in. (incremental)
Optigraph target 10	529.0	681.0	-----do-----	0.0204 in./in.	^b ± 0.46 in.
Optigraph target 11	370.4	517.5	-----do-----	0.0283 in./in.	± 0.46
Optigraph target 12	412.4	517.5	-----do-----	0.0272 in./in.	± 0.46
Optigraph target 13	273.1	383.0	-----do-----	0.0230 in./in.	± 0.46
Optigraph target 14	331.0	389.0	-----do-----	0.0212 in./in.	± 0.46
Optigraph target 15	155.2	208.5	-----do-----	0.0165 in./in.	± 0.46
Optigraph target 16	231.0	211.5	-----do-----	0.0152 in./in.	± 0.46

^aRead manually as slope of velocity trace.

^bAbsolute from ground zero.

TABLE 3.- ZERO-LIFT PLUS DROOP WING DEFLECTION COEFFICIENT $Z_0 + Z_1$

Flight	Run	Zero-lift plus droop wing deflection coefficient, in., at target -					
		9	10	11	12	13	14
8	15	21.897	22.727	13.100	13.009	7.300	8.020
10	17	23.047	24.464	13.316	14.388	7.387	8.560
10	18	23.339	24.695	13.464	14.517	7.504	8.623
12	14	19.205	20.544	11.986	12.283	7.130	7.554

TABLE 4.- AILERON WING DEFLECTION COEFFICIENT Z_{6AIL}

Flight	Run	Aileron wing deflection coefficient, in./deg, at target -					
		9	10	11	12	13	14
8	15	0.368	0.492	0.179	0.209	0.054	0.093
10	17	.494	.578	.237	.296	.096	.143
10	18	.424	.528	.206	.255	.076	.121
12	14	.308	.359	.145	.181	.059	.087

TABLE 5.- WING-FLAPPING WING DEFLECTION COEFFICIENT

Flight	Run	Wing-flapping wing deflection coefficient, in./nT _F , at target -					
		9	10	11	12	13	14
8	15	-2.219	-2.136	-1.176	-1.241	-0.493	-0.614
10	17	-2.218	-2.247	-1.190	-1.349	-.510	-.695
10	18	-2.131	-2.225	-1.113	-1.196	-.461	-.629
12	14	-2.310	-2.194	-1.269	-1.342	-.560	-.667

TABLE 6.- SIDESLIP WING DEFLECTION COEFFICIENT $Z_{n\beta}$

Flight	Run	Sideslip wing deflection coefficient, in./deg, at target -					
		9	10	11	12	13	14
8	15	0.111	0.128	0.074	0.074	0.035	0.049
10	17	.163	.192	.111	.122	.048	.029
10	18	.152	.157	.094	.094	.037	.042
12	14	.126	.073	.065	.076	.009	.031

TABLE 7.- ROLLING-VELOCITY WING DEFLECTION COEFFICIENT Z_p

Flight	Run	Rolling-velocity wing deflection coefficient, in./radian/sec, at target -					
		9	10	11	12	13	14
8	15	-2.540	-5.252	-1.278	-1.482	-0.387	-0.999
10	17	-2.346	-2.674	-1.255	-1.505	-.788	-.753
10	18	-1.411	-2.708	-.872	-1.259	-.317	-.633
12	14	-1.283	-1.777	-.797	-1.102	-.524	-.681

TABLE 8.- TYPICAL TARGET DEFLECTIONS AND STANDARD ERROR FOR FLIGHT 10, RUN 17, LEFT ROLL

Target	Target deflection coefficient and standard error for -					
	$S_{Z'}'_{roll}$ (a)	$Z_0 + Z_1$	$Z_{\delta_{AIL}}$	Z_{nT_F}	$Z_{n\beta}$	Z_p
9	± 0.176	23.047 ± 0.053	0.494 ± 0.011	-2.218 ± 0.065	0.163 ± 0.022	-2.346 ± 0.342
10	± 0.337	24.464 ± 0.100	0.578 ± 0.022	-2.247 ± 0.122	0.192 ± 0.042	-2.674 ± 0.651
11	± 0.100	13.316 ± 0.029	0.237 ± 0.005	-1.190 ± 0.035	0.111 ± 0.011	-1.255 ± 0.192
12	± 0.161	14.388 ± 0.047	0.296 ± 0.010	-1.349 ± 0.057	0.122 ± 0.019	-1.505 ± 0.309
13	± 0.071	7.387 ± 0.020	0.096 ± 0.004	-0.510 ± 0.025	0.048 ± 0.008	-0.788 ± 0.137
14	± 0.081	8.560 ± 0.023	0.143 ± 0.004	-0.695 ± 0.029	0.029 ± 0.010	-0.753 ± 0.156

^aStandard error of the equation for each target calculated by method of appendix A.

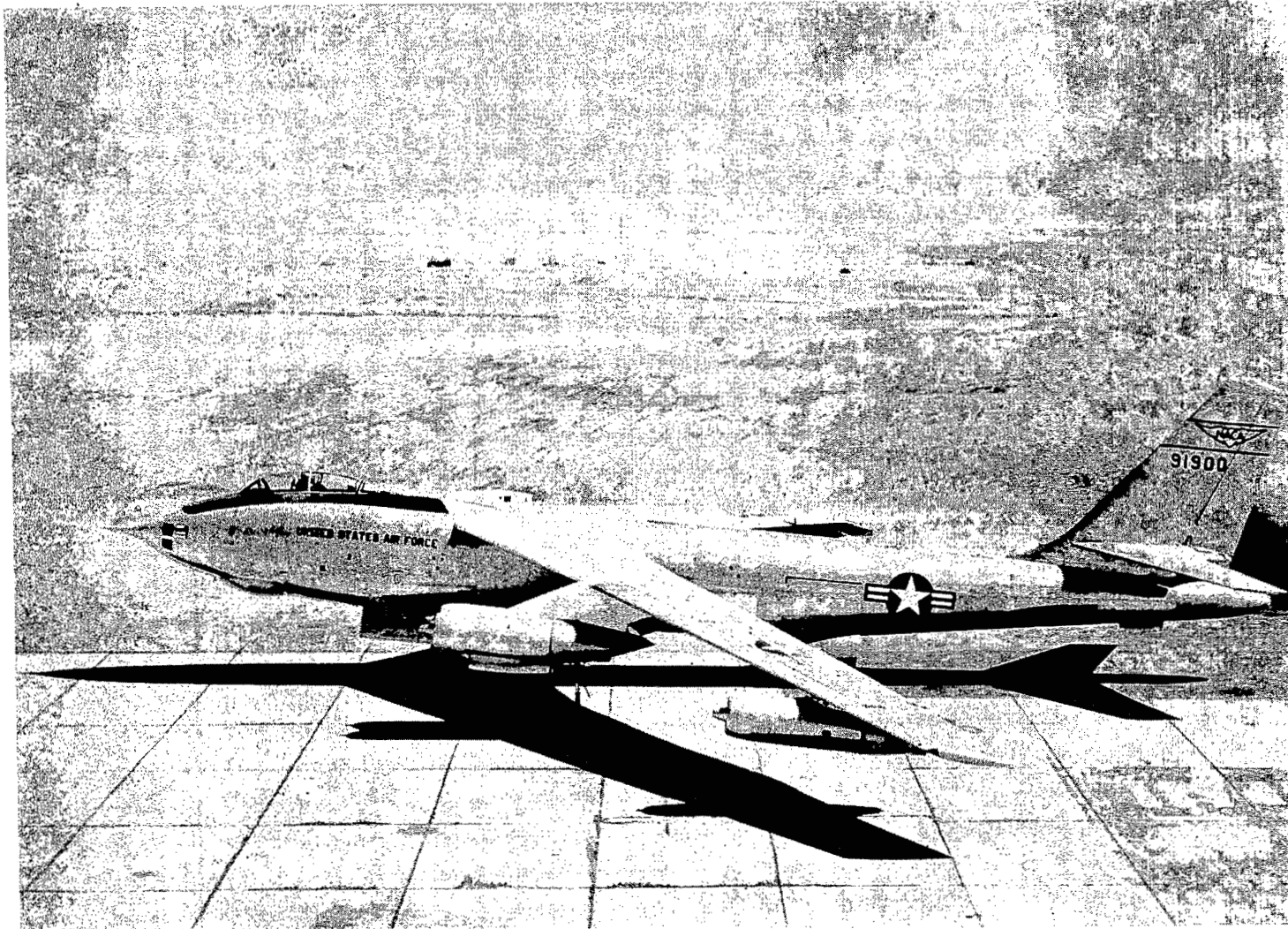


Figure 1.- Photograph of test airplane. L-86692

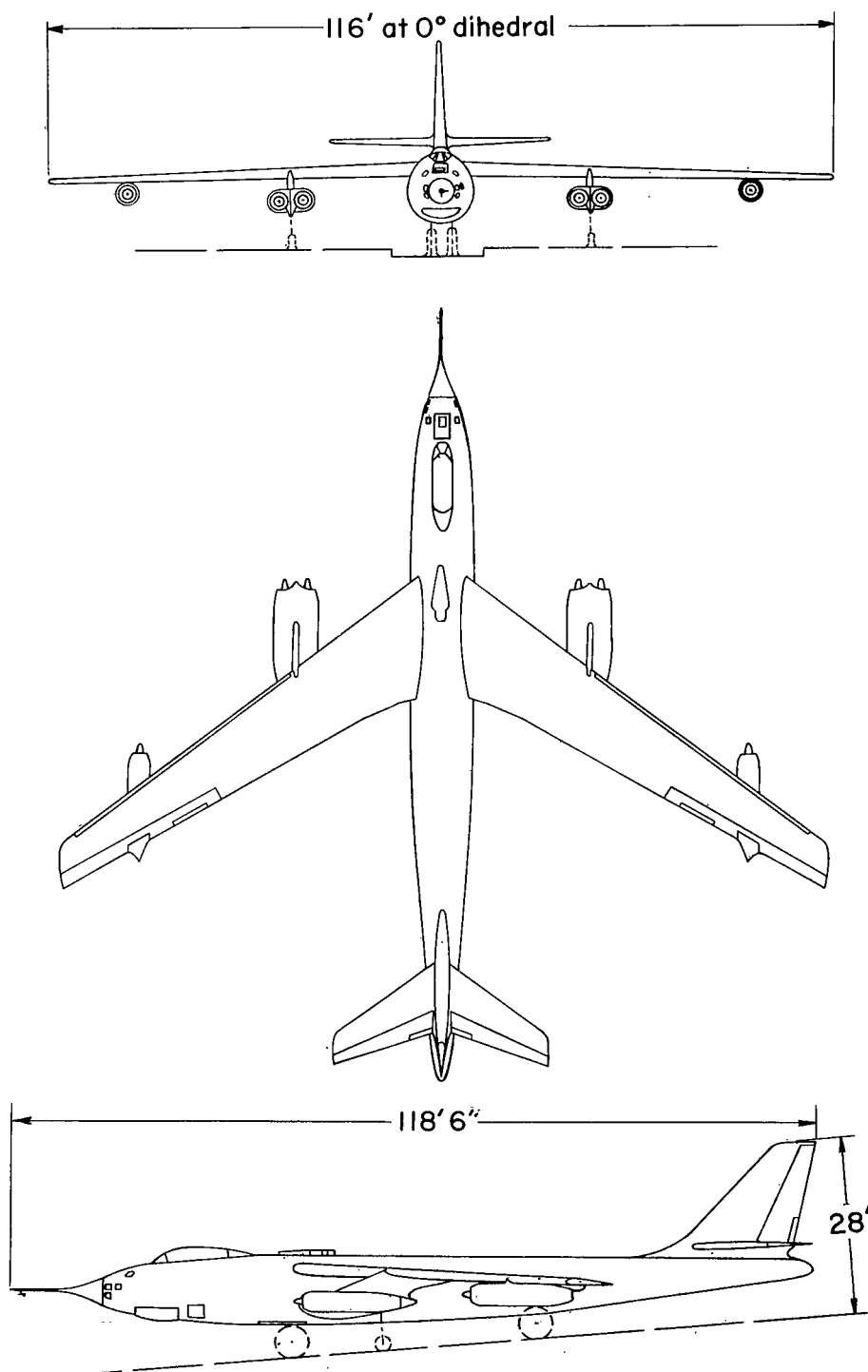


Figure 2.- Three views of test airplane.

Optigraph-target locations		
Target no.	X	Y
9	474.5	681.0
10	529.0	681.0
11	370.4	517.5
12	412.4	517.5
13	273.1	383.0
14	331.0	389.0
15	155.2	208.5
16	231.0	211.5

Optigraph-camera location		
Camera	X	Y
I	46.0	3.0

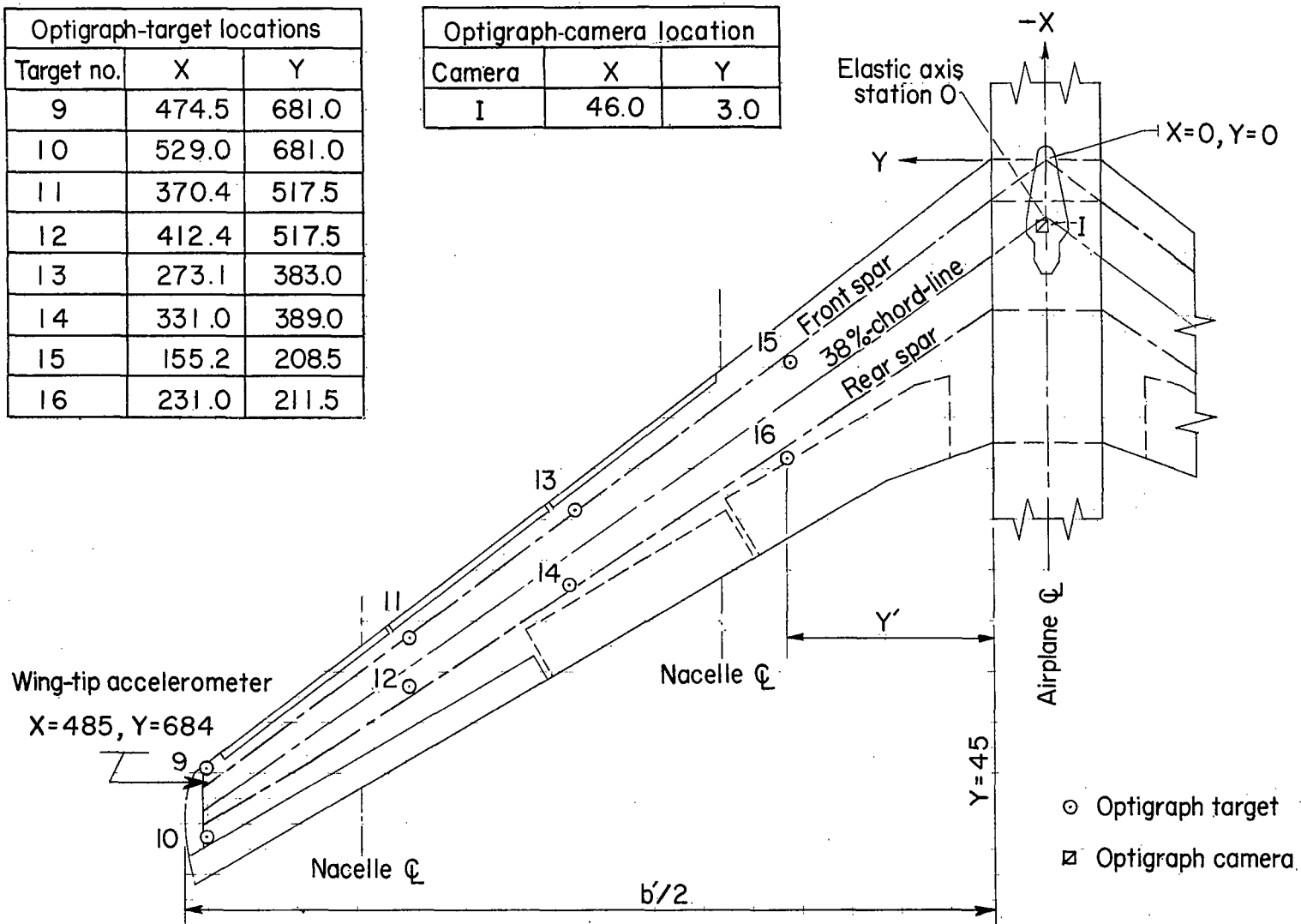


Figure 3.- Location of optigraph camera and targets used during test.
All dimensions are given in inches.

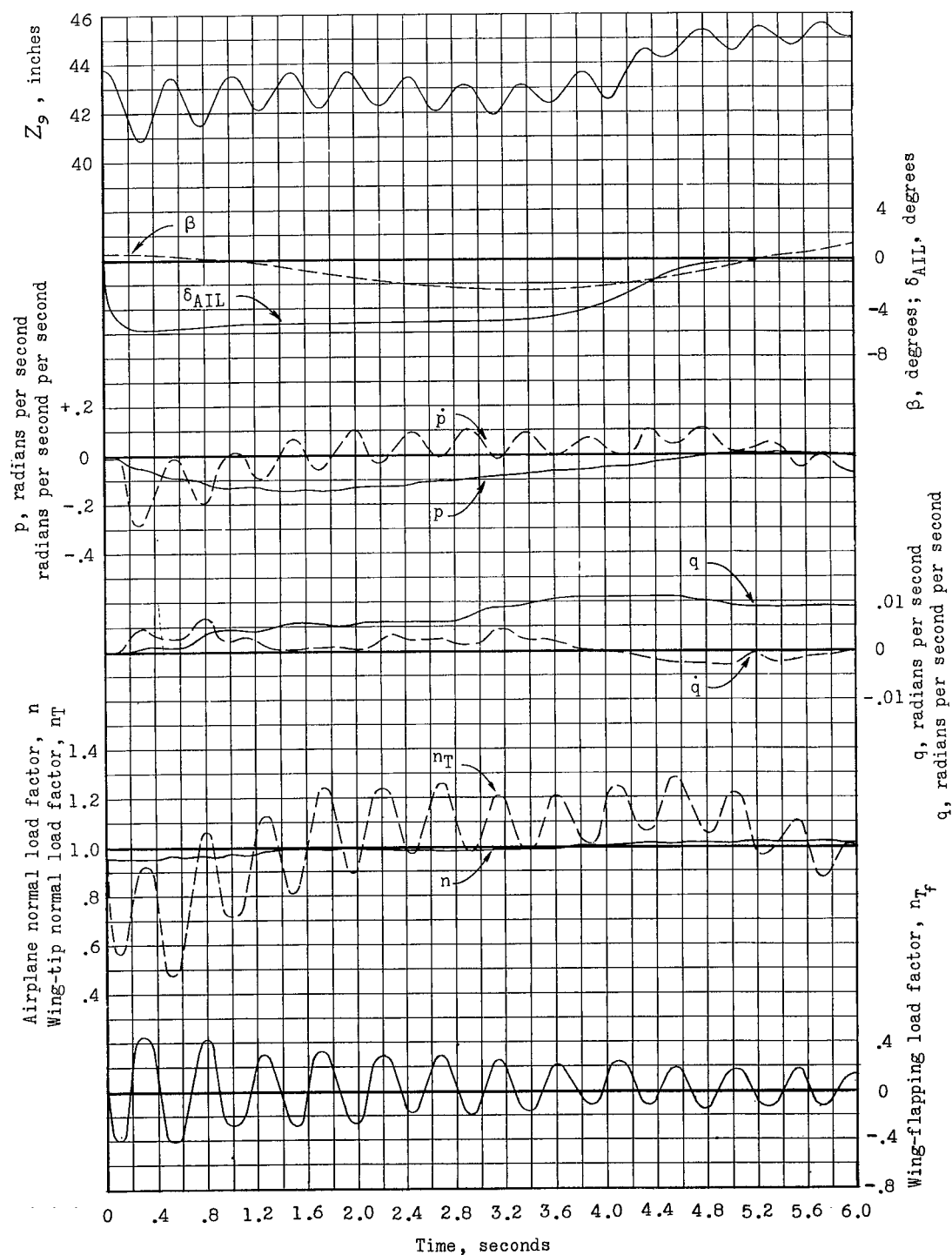


Figure 4.- Time-history data for flight 8, run 15, left roll, Mach number 0.60, altitude 34,500 feet.

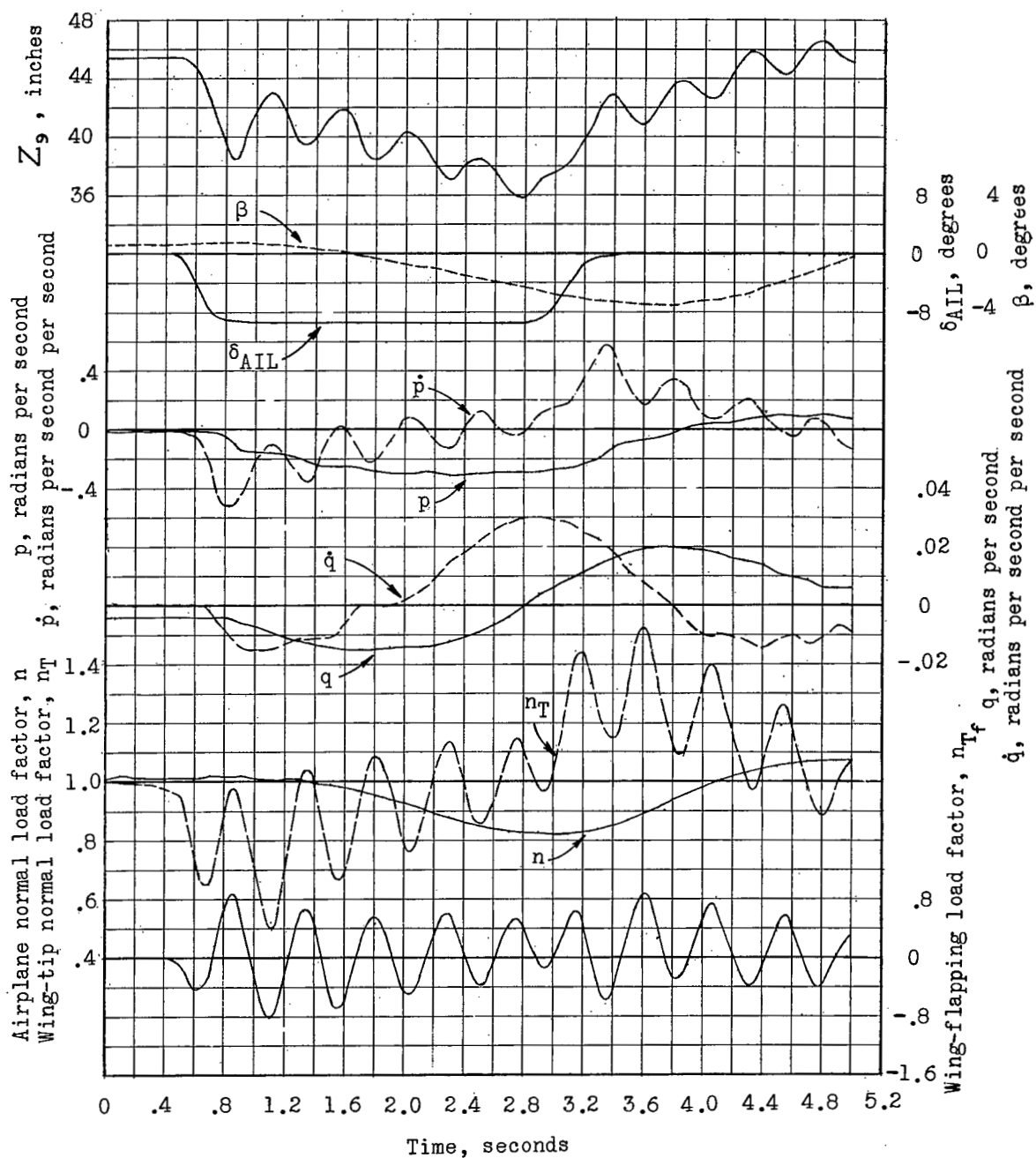


Figure 5.- Time-history data for flight 10, run 17, left roll, Mach number 0.71, altitude 34,900 feet.

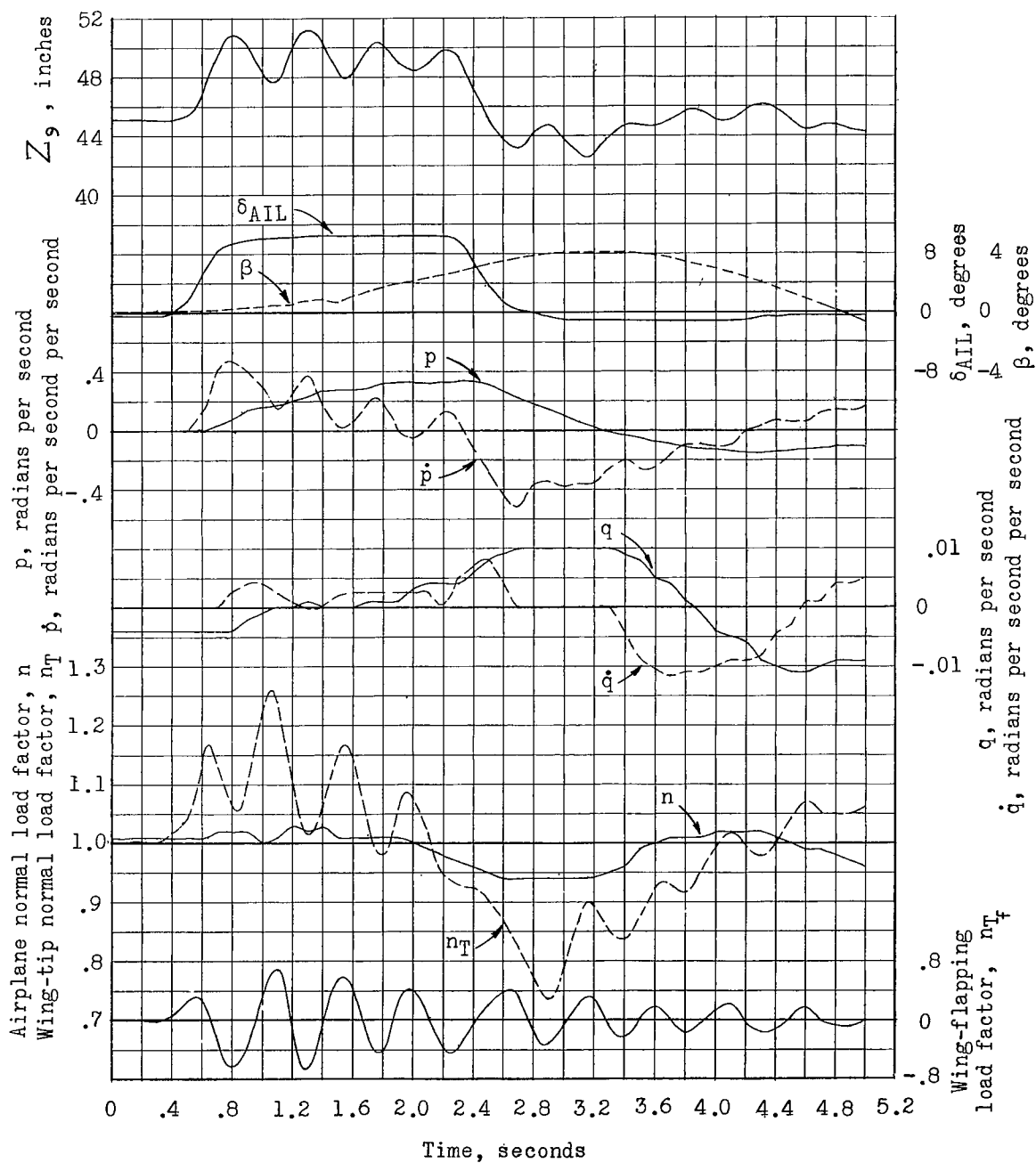


Figure 6.- Time-history data for flight 10, run 18, right roll, Mach number 0.71, altitude 35,300 feet.

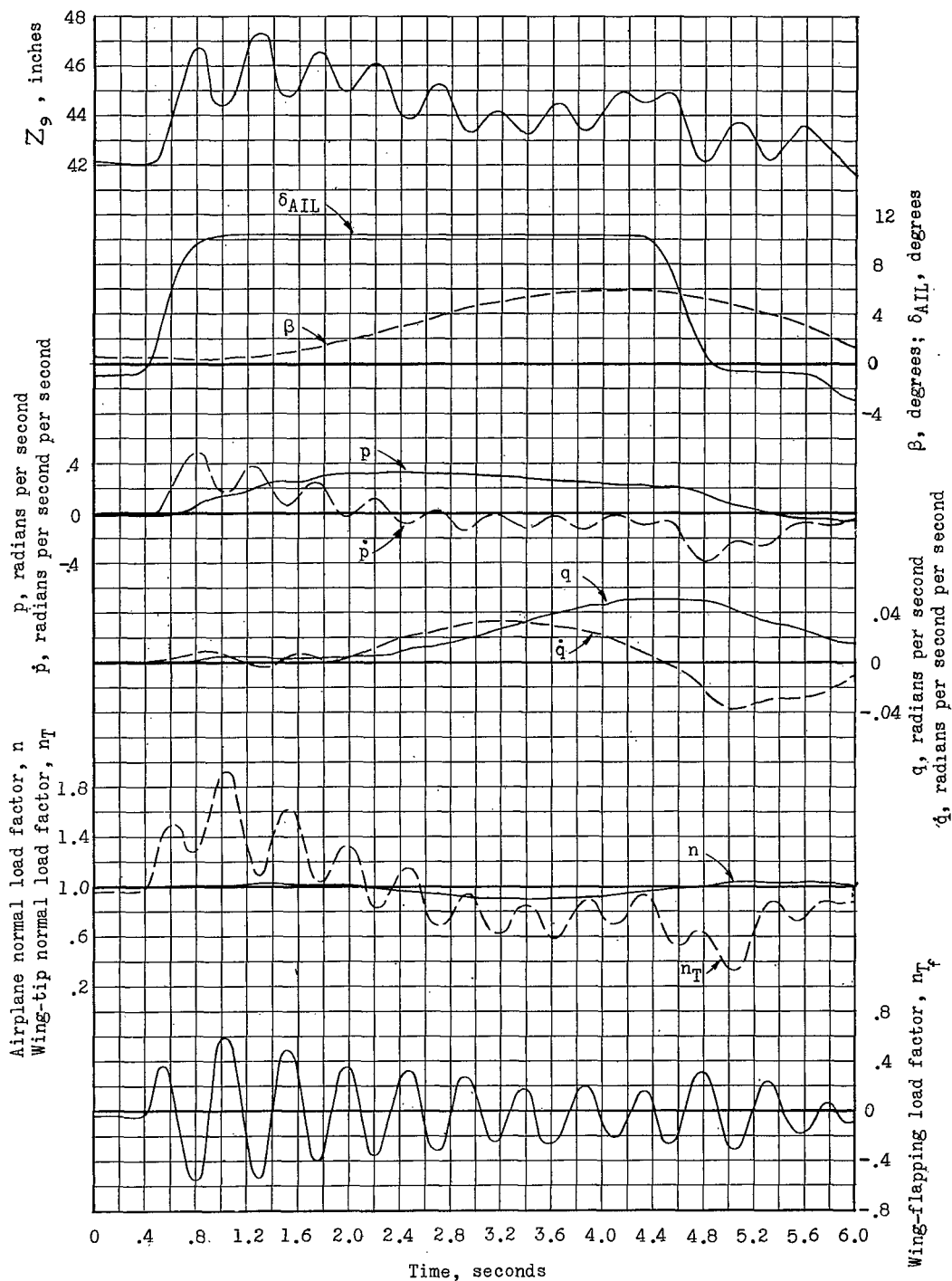


Figure 7.- Time-history data for flight 12, run 14, right roll, Mach number 0.60, altitude, 34,800 feet.

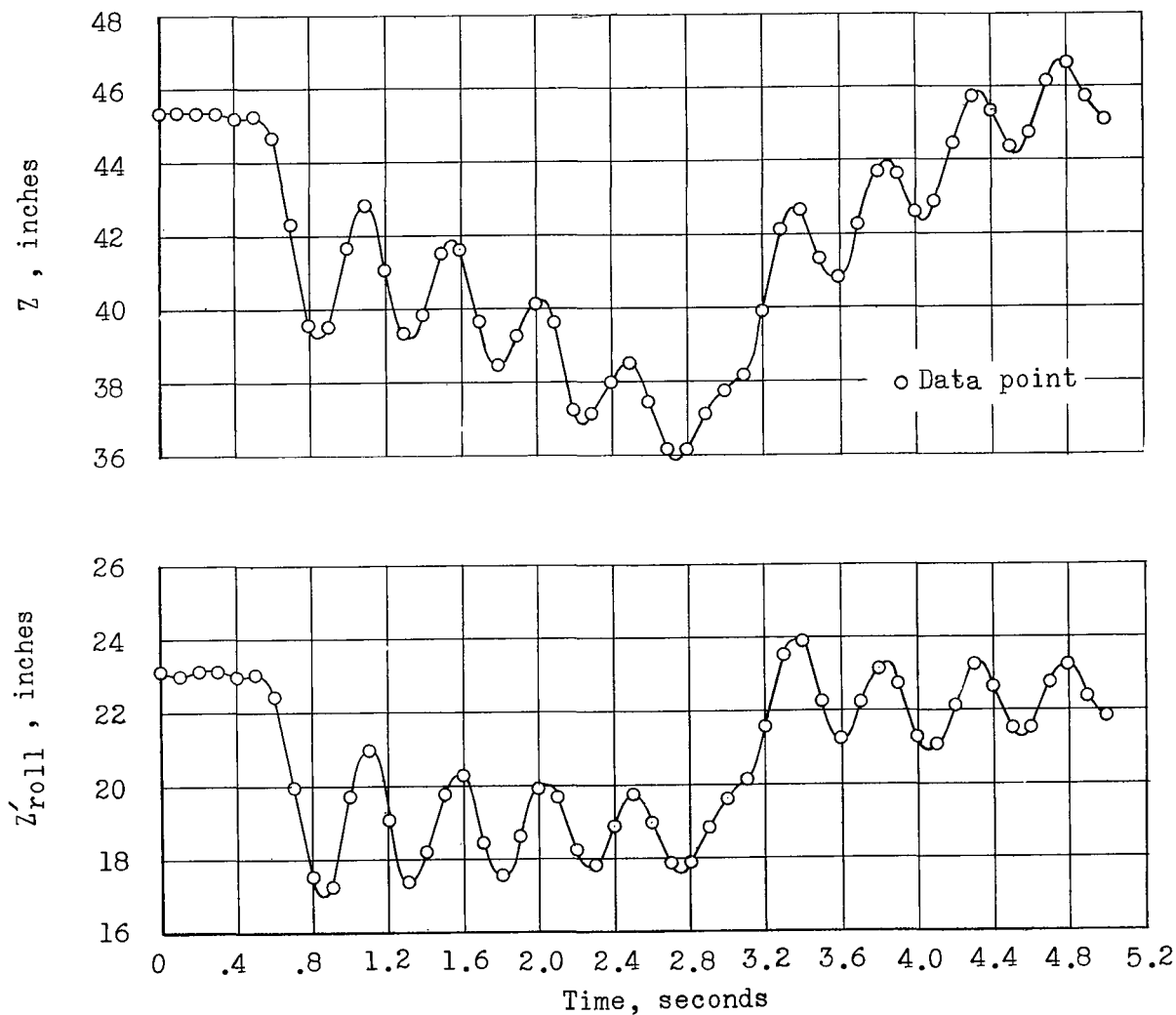


Figure 8.- Typical time history of target 9 deflection data, before and after symmetrical deflections were removed, showing 51 data points used in analysis.

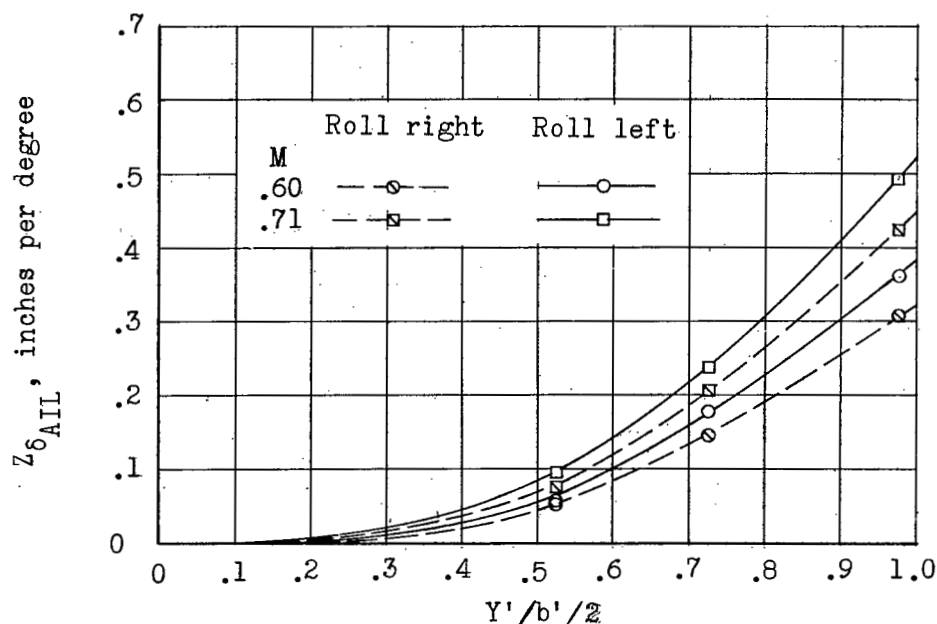


Figure 9.- Flight-test front-spar deflections due to aileron deflection of 1° , altitude approximately 35,000 feet. (See table 1.)

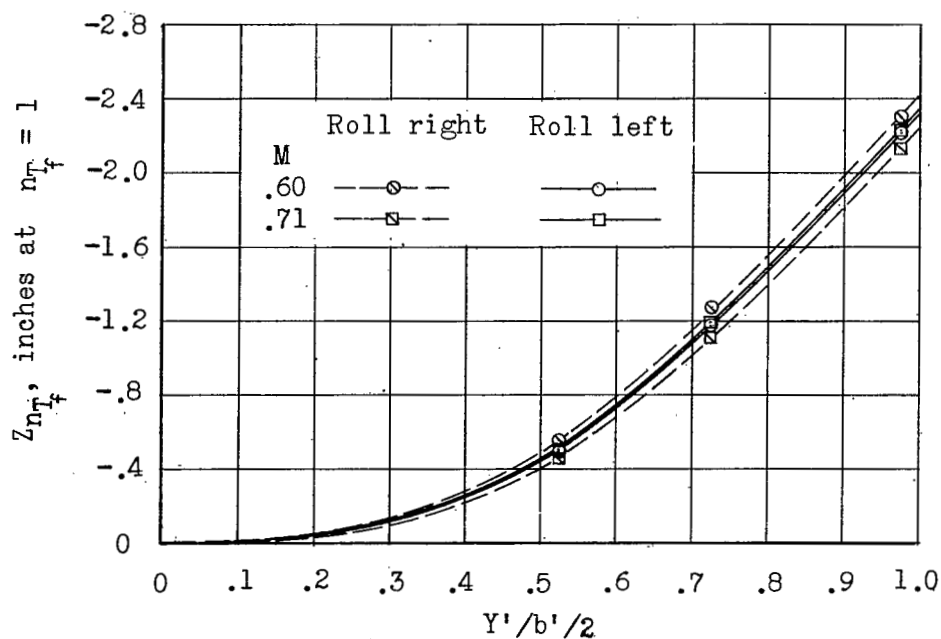


Figure 10.- Flight-test front-spar deflections due to wing-flapping load factor, $n_{T_f} = 1$, altitude approximately 35,000 feet. (See table 1.)

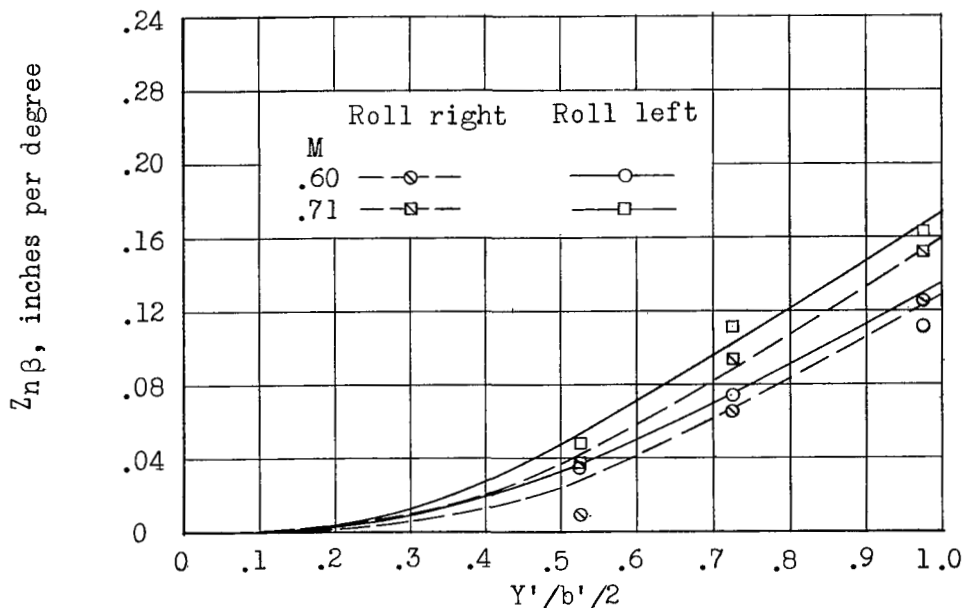


Figure 11.- Flight-test front-spar sideslip deflection per $n\beta$, altitude approximately 35,000 feet. (See table 1.)

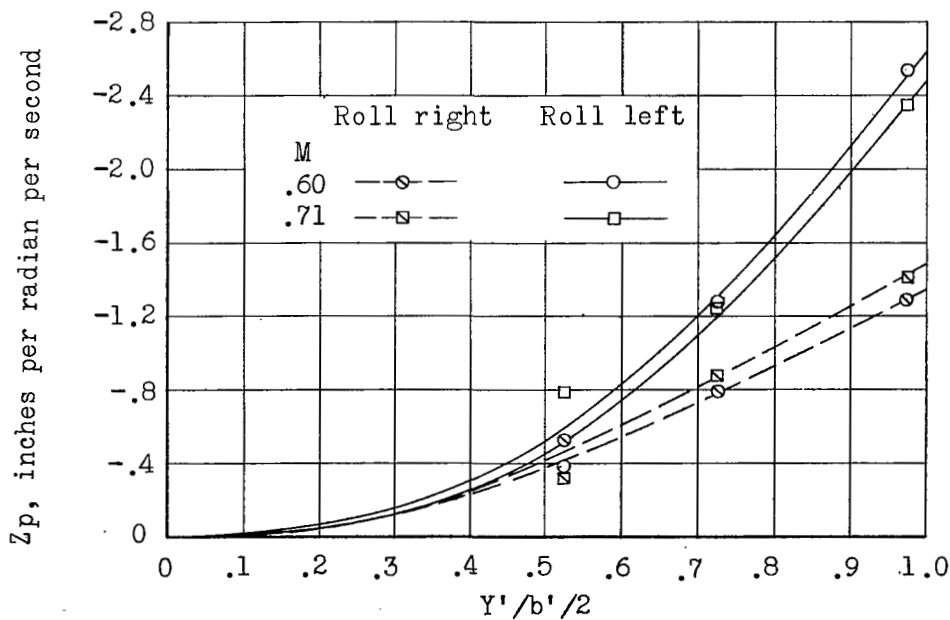


Figure 12.- Flight-test front-spar deflection due to rolling velocity of one radian per second, altitude approximately 35,000 feet. (See table 1.)

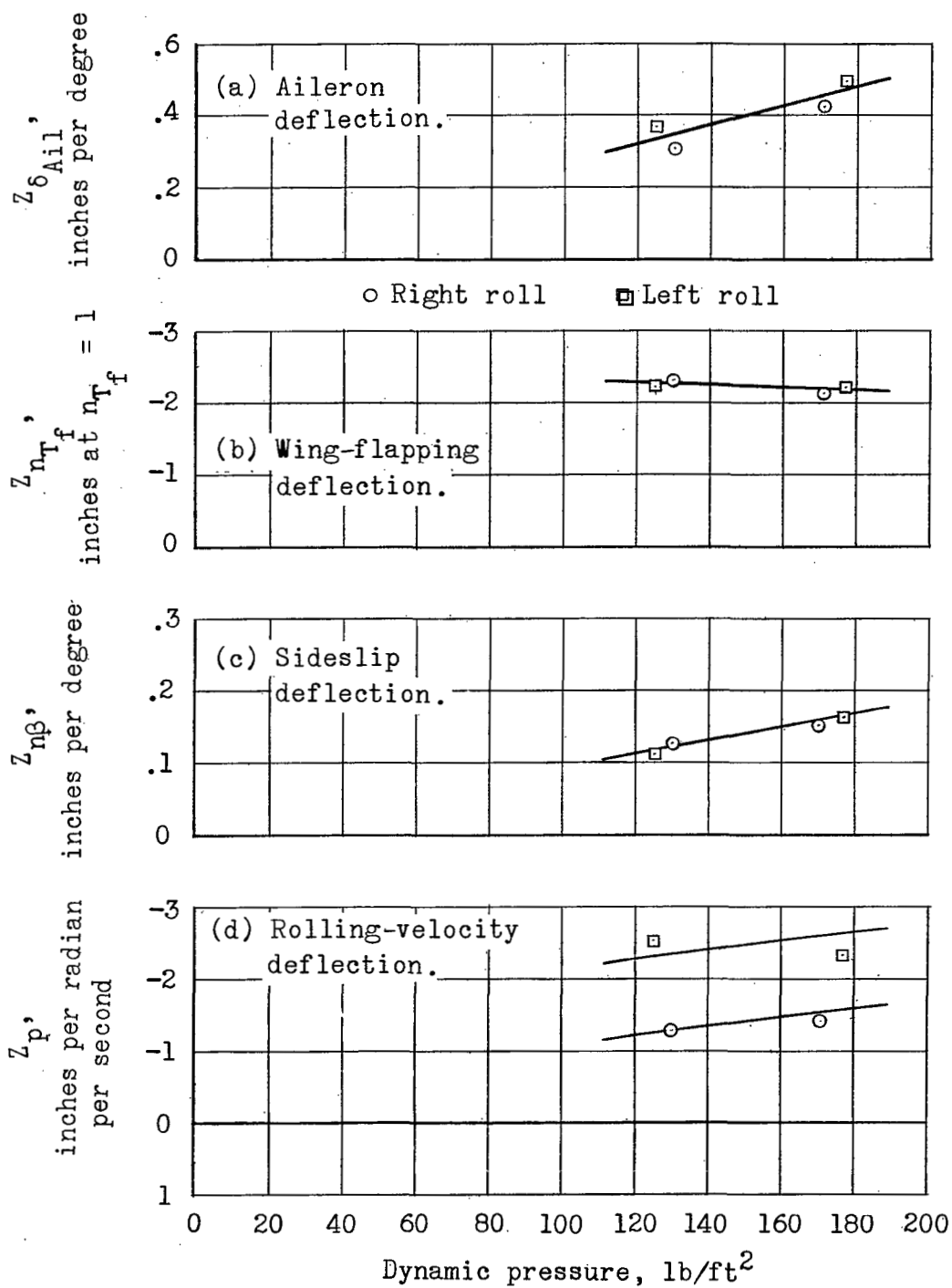


Figure 13.- Variation of left wing tip, target 9, deflection coefficients with dynamic pressure.

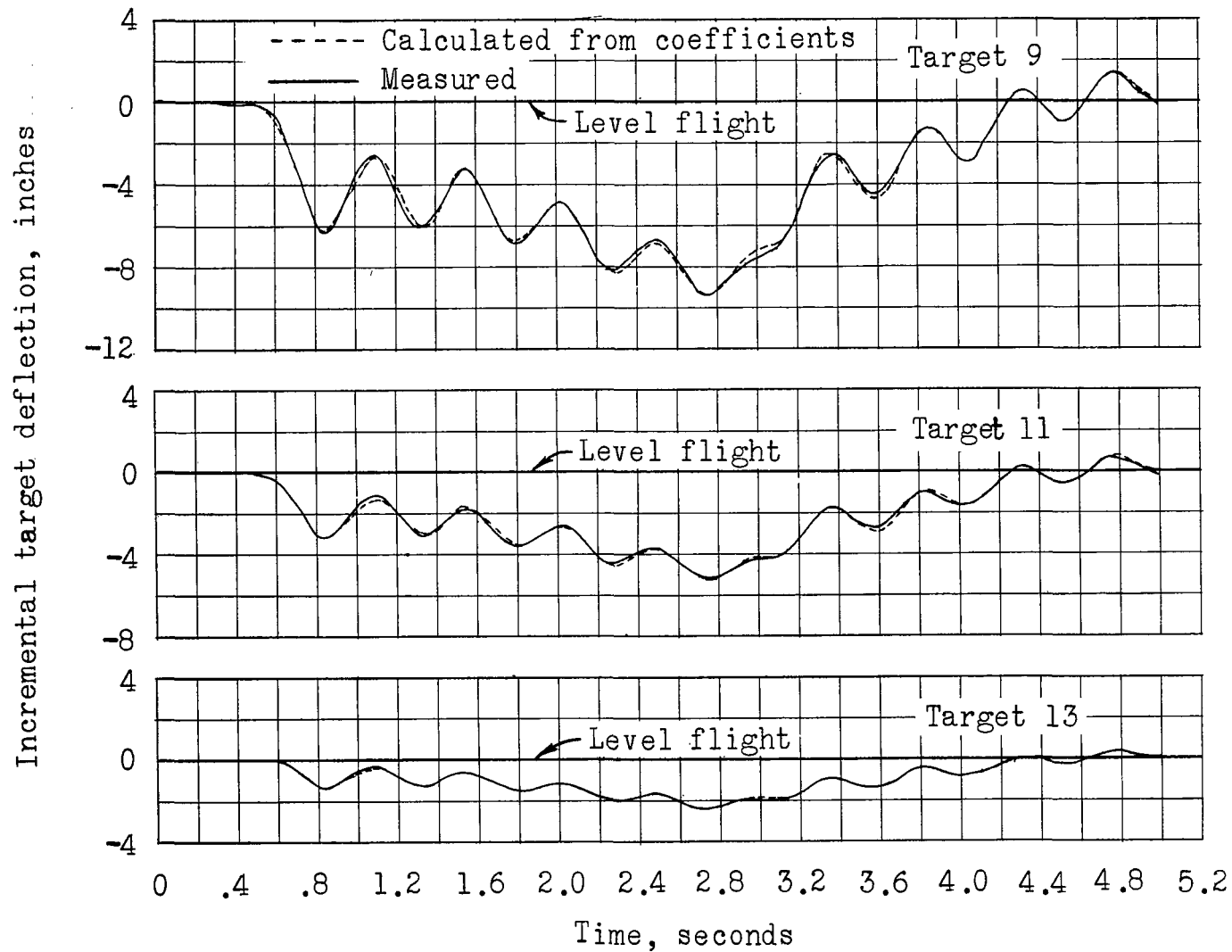


Figure 14.- Time-history comparison of measured and calculated target deflections about 1g level-flight condition.

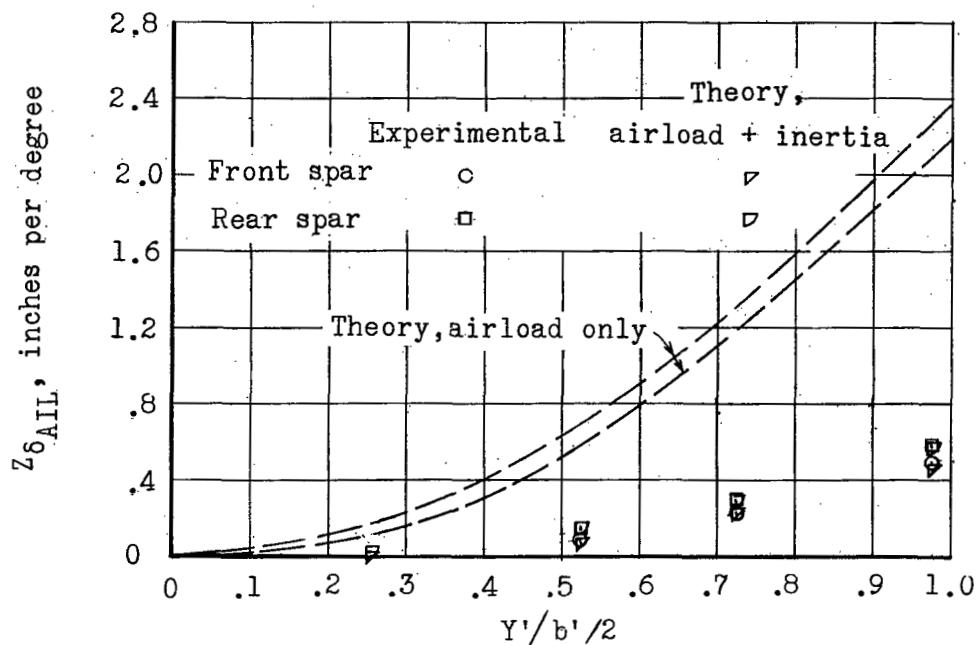


Figure 15.- Comparison of experimental and theoretical aileron wing deflection coefficients.

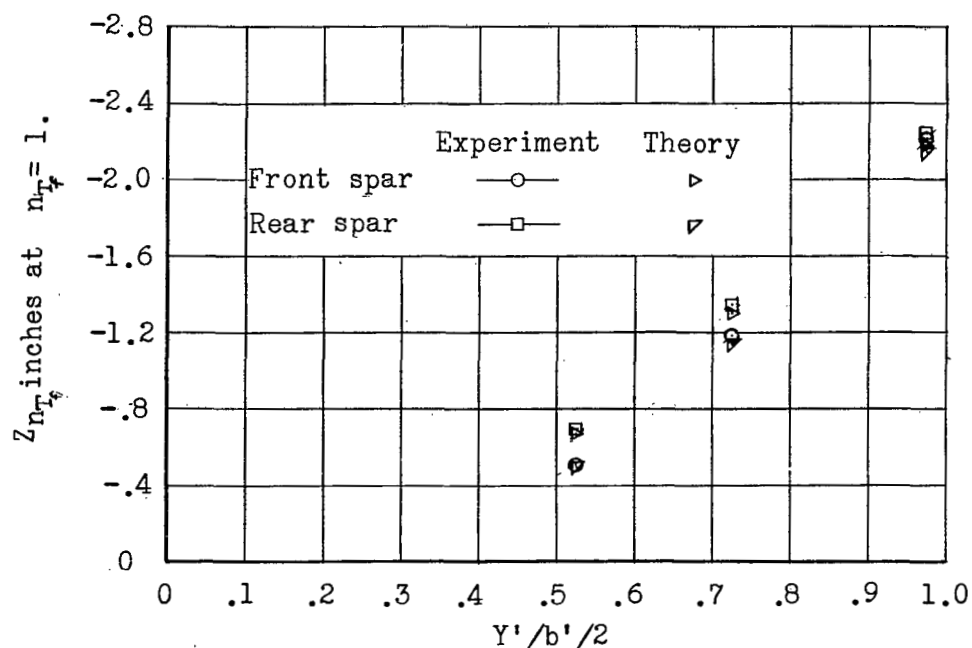


Figure 16.- Comparison of experimental and theoretical wing-flapping deflection coefficients.

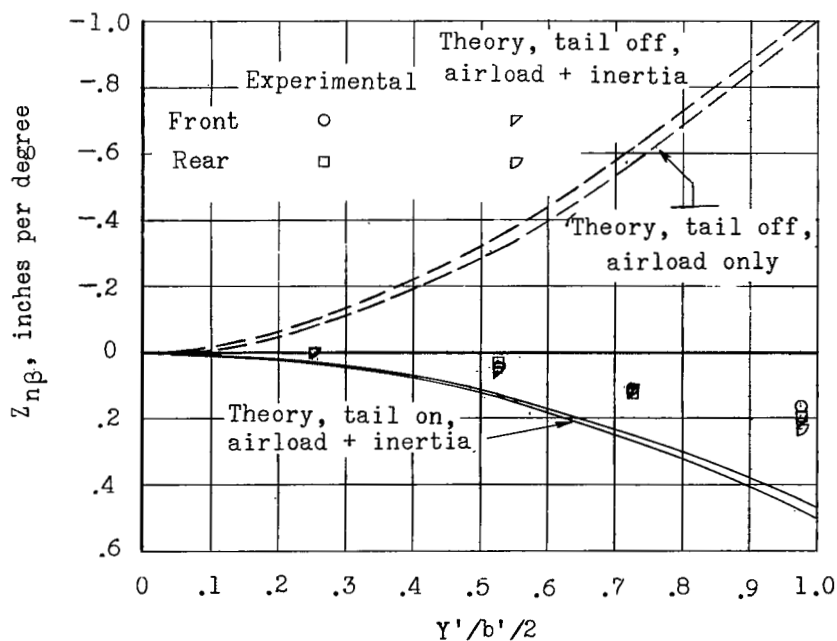


Figure 17.- Comparison of experimental and theoretical sideslip wing deflection coefficients.

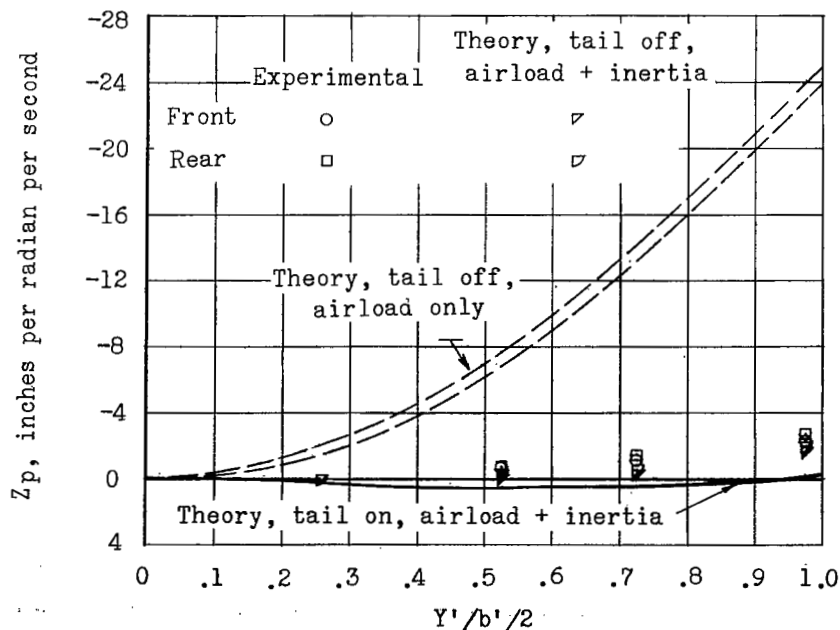


Figure 18.- Comparison of experimental and theoretical rolling-velocity wing deflection coefficients.

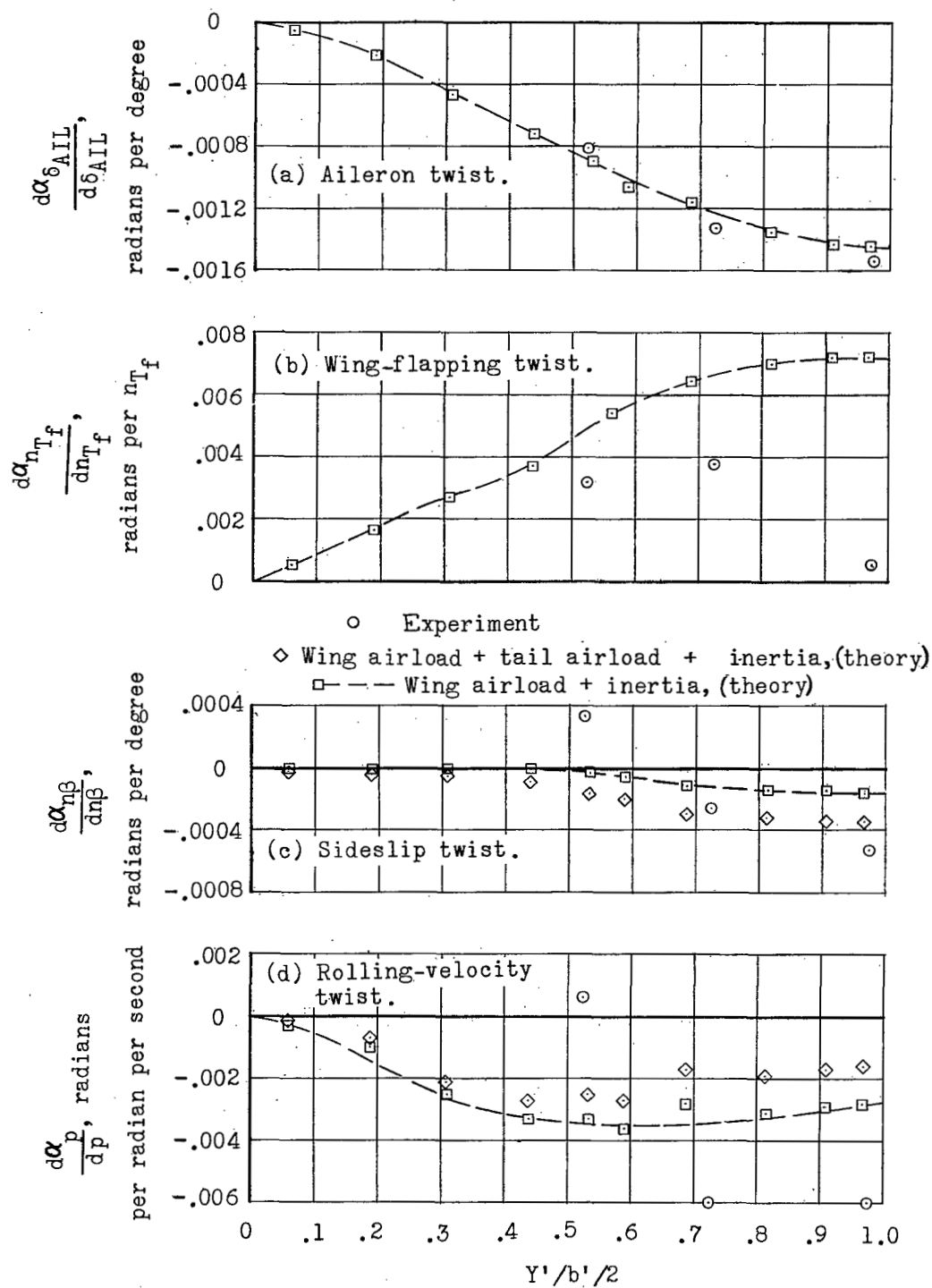


Figure 19.- Comparison of experimental and theoretical streamwise wing twist.

[REDACTED]



3 1176 01437 2123



1
2

[REDACTED]